MICROLITHOGRAPHY

Science and Technology

Second Edition

OPTICAL SCIENCE AND ENGINEERING

Founding Editor
Brian J. Thompson
University of Rochester
Rochester, New York

1. Electron and Ion Microscopy and Microanalysis: Principles and Applications, *Lawrence E. Murr*
2. Acousto-Optic Signal Processing: Theory and Implementation, *edited by Norman J. Berg and John N. Lee*
3. Electro-Optic and Acousto-Optic Scanning and Deflection, *Milton Gottlieb, Clive L. M. Ireland, and John Martin Ley*
4. Single-Mode Fiber Optics: Principles and Applications, *Luc B. Jeunhomme*
5. Pulse Code Formats for Fiber Optical Data Communication: Basic Principles and Applications, *David J. Morris*
6. Optical Materials: An Introduction to Selection and Application, *Solomon Musikant*
7. Infrared Methods for Gaseous Measurements: Theory and Practice, *edited by Joda Wormhoudt*
8. Laser Beam Scanning: Opto-Mechanical Devices, Systems, and Data Storage Optics, *edited by Gerald F. Marshall*
9. Opto-Mechanical Systems Design, *Paul R. Yoder, Jr.*
10. Optical Fiber Splices and Connectors: Theory and Methods, *Calvin M. Miller with Stephen C. Mettler and Ian A. White*
11. Laser Spectroscopy and Its Applications, *edited by Leon J. Radziemski, Richard W. Solarz, and Jeffrey A. Paisner*
12. Infrared Optoelectronics: Devices and Applications, *William Nunley and J. Scott Bechtel*
13. Integrated Optical Circuits and Components: Design and Applications, *edited by Lynn D. Hutcheson*
14. Handbook of Molecular Lasers, *edited by Peter K. Cheo*
15. Handbook of Optical Fibers and Cables, *Hiroshi Murata*
16. Acousto-Optics, *Adrian Korpel*
17. Procedures in Applied Optics, *John Strong*
18. Handbook of Solid-State Lasers, *edited by Peter K. Cheo*
19. Optical Computing: Digital and Symbolic, *edited by Raymond Arrathoon*
20. Laser Applications in Physical Chemistry, *edited by D. K. Evans*
21. Laser-Induced Plasmas and Applications, *edited by Leon J. Radziemski and David A. Cremers*
22. Infrared Technology Fundamentals, *Irving J. Spiro and Monroe Schlessinger*
23. Single-Mode Fiber Optics: Principles and Applications, Second Edition, Revised and Expanded, *Luc B. Jeunhomme*
24. Image Analysis Applications, *edited by Rangachar Kasturi and Mohan M. Trivedi*
25. Photoconductivity: Art, Science, and Technology, *N. V. Joshi*
26. Principles of Optical Circuit Engineering, *Mark A. Mentzer*
27. Lens Design, *Milton Laikin*

28. Optical Components, Systems, and Measurement Techniques, *Rajpal S. Sirohi and M. P. Kothiyal*
29. Electron and Ion Microscopy and Microanalysis: Principles and Applications, Second Edition, Revised and Expanded, *Lawrence E. Murr*
30. Handbook of Infrared Optical Materials, *edited by Paul Klocek*
31. Optical Scanning, *edited by Gerald F. Marshall*
32. Polymers for Lightwave and Integrated Optics: Technology and Applications, *edited by Lawrence A. Hornak*
33. Electro-Optical Displays, *edited by Mohammad A. Karim*
34. Mathematical Morphology in Image Processing, *edited by Edward R. Dougherty*
35. Opto-Mechanical Systems Design: Second Edition, Revised and Expanded, *Paul R. Yoder, Jr.*
36. Polarized Light: Fundamentals and Applications, *Edward Collett*
37. Rare Earth Doped Fiber Lasers and Amplifiers, *edited by Michel J. F. Digonnet*
38. Speckle Metrology, *edited by Rajpal S. Sirohi*
39. Organic Photoreceptors for Imaging Systems, *Paul M. Borsenberger and David S. Weiss*
40. Photonic Switching and Interconnects, *edited by Abdellatif Marrakchi*
41. Design and Fabrication of Acousto-Optic Devices, *edited by Akis P. Goutzoulis and Dennis R. Pape*
42. Digital Image Processing Methods, *edited by Edward R. Dougherty*
43. Visual Science and Engineering: Models and Applications, *edited by D. H. Kelly*
44. Handbook of Lens Design, *Daniel Malacara and Zacarias Malacara*
45. Photonic Devices and Systems, *edited by Robert G. Hunsberger*
46. Infrared Technology Fundamentals: Second Edition, Revised and Expanded, *edited by Monroe Schlessinger*
47. Spatial Light Modulator Technology: Materials, Devices, and Applications, *edited by Uzi Efron*
48. Lens Design: Second Edition, Revised and Expanded, *Milton Laikin*
49. Thin Films for Optical Systems, *edited by Francoise R. Flory*
50. Tunable Laser Applications, *edited by F. J. Duarte*
51. Acousto-Optic Signal Processing: Theory and Implementation, Second Edition, *edited by Norman J. Berg and John M. Pellegrino*
52. Handbook of Nonlinear Optics, *Richard L. Sutherland*
53. Handbook of Optical Fibers and Cables: Second Edition, *Hiroshi Murata*
54. Optical Storage and Retrieval: Memory, Neural Networks, and Fractals, *edited by Francis T. S. Yu and Suganda Jutamulia*
55. Devices for Optoelectronics, *Wallace B. Leigh*
56. Practical Design and Production of Optical Thin Films, *Ronald R. Willey*
57. Acousto-Optics: Second Edition, *Adrian Korpel*
58. Diffraction Gratings and Applications, *Erwin G. Loewen and Evgeny Popov*
59. Organic Photoreceptors for Xerography, *Paul M. Borsenberger and David S. Weiss*
60. Characterization Techniques and Tabulations for Organic Nonlinear Optical Materials, *edited by Mark G. Kuzyk and Carl W. Dirk*
61. Interferogram Analysis for Optical Testing, *Daniel Malacara, Manuel Servin, and Zacarias Malacara*
62. Computational Modeling of Vision: The Role of Combination, *William R. Uttal, Ramakrishna Kakarala, Spiram Dayanand, Thomas Shepherd, Jagadeesh Kalki, Charles F. Lunskis, Jr., and Ning Liu*
63. Microoptics Technology: Fabrication and Applications of Lens Arrays and Devices, *Nicholas Borrelli*
64. Visual Information Representation, Communication, and Image Processing, *edited by Chang Wen Chen and Ya-Qin Zhang*
65. Optical Methods of Measurement, *Rajpal S. Sirohi and F. S. Chau*

66. Integrated Optical Circuits and Components: Design and Applications, *edited by Edmond J. Murphy*
67. Adaptive Optics Engineering Handbook, *edited by Robert K. Tyson*
68. Entropy and Information Optics, *Francis T. S. Yu*
69. Computational Methods for Electromagnetic and Optical Systems, *John M. Jarem and Partha P. Banerjee*
70. Laser Beam Shaping, *Fred M. Dickey and Scott C. Holswade*
71. Rare-Earth-Doped Fiber Lasers and Amplifiers: Second Edition, Revised and Expanded, *edited by Michel J. F. Digonnet*
72. Lens Design: Third Edition, Revised and Expanded, *Milton Laikin*
73. Handbook of Optical Engineering, *edited by Daniel Malacara and Brian J. Thompson*
74. Handbook of Imaging Materials: Second Edition, Revised and Expanded, *edited by Arthur S. Diamond and David S. Weiss*
75. Handbook of Image Quality: Characterization and Prediction, *Brian W. Keelan*
76. Fiber Optic Sensors, *edited by Francis T. S. Yu and Shizhuo Yin*
77. Optical Switching/Networking and Computing for Multimedia Systems, *edited by Mohsen Guizani and Abdella Battou*
78. Image Recognition and Classification: Algorithms, Systems, and Applications, *edited by Bahram Javidi*
79. Practical Design and Production of Optical Thin Films: Second Edition, Revised and Expanded, *Ronald R. Willey*
80. Ultrafast Lasers: Technology and Applications, *edited by Martin E. Fermann, Almantas Galvanauskas, and Gregg Sucha*
81. Light Propagation in Periodic Media: Differential Theory and Design, *Michel Nevière and Evgeny Popov*
82. Handbook of Nonlinear Optics, Second Edition, Revised and Expanded, *Richard L. Sutherland*
83. Polarized Light: Second Edition, Revised and Expanded, *Dennis Goldstein*
84. Optical Remote Sensing: Science and Technology, *Walter Egan*
85. Handbook of Optical Design: Second Edition, *Daniel Malacara and Zacarías Malacara*
86. Nonlinear Optics: Theory, Numerical Modeling, and Applications, *Partha P. Banerjee*
87. Semiconductor and Metal Nanocrystals: Synthesis and Electronic and Optical Properties, edited by *Victor I. Klimov*
88. High-Performance Backbone Network Technology, *edited by Naoaki Yamanaka*
89. Semiconductor Laser Fundamentals, *Toshiaki Suhara*
90. Handbook of Optical and Laser Scanning, *edited by Gerald F. Marshall*
91. Organic Light-Emitting Diodes: Principles, Characteristics, and Processes, *Jan Kalinowski*
92. Micro-Optomechatronics, *Hiroshi Hosaka, Yoshitada Katagiri, Terunao Hirota, and Kiyoshi Itao*
93. Microoptics Technology: Second Edition, *Nicholas F. Borrelli*
94. Organic Electroluminescence, *edited by Zakya Kafafi*
95. Engineering Thin Films and Nanostructures with Ion Beams, *Emile Knystautas*
96. Interferogram Analysis for Optical Testing, Second Edition, *Daniel Malacara, Manuel Sercin, and Zacarias Malacara*
97. Laser Remote Sensing, *edited by Takashi Fujii and Tetsuo Fukuchi*
98. Passive Micro-Optical Alignment Methods, *edited by Robert A. Boudreau and Sharon M. Boudreau*
99. Organic Photovoltaics: Mechanism, Materials, and Devices, *edited by Sam-Shajing Sun and Niyazi Serdar Sariciftci*
100. Handbook of Optical Interconnects, *edited by Shigeru Kawai*
101. GMPLS Technologies: Broadband Backbone Networks and Systems, *Naoaki Yamanaka, Kohei Shiomoto, and Eiji Oki*

102. Laser Beam Shaping Applications, *edited by Fred M. Dickey, Scott C. Holswade and David L. Shealy*
103. Electromagnetic Theory and Applications for Photonic Crystals, *Kiyotoshi Yasumoto*
104. Physics of Optoelectronics, *Michael A. Parker*
105. Opto-Mechanical Systems Design: Third Edition, *Paul R. Yoder, Jr.*
106. Color Desktop Printer Technology, *edited by Mitchell Rosen and Noboru Ohta*
107. Laser Safety Management, *Ken Barat*
108. Optics in Magnetic Multilayers and Nanostructures, *Štefan Višňovský*
109. Optical Inspection of Microsystems, *edited by Wolfgang Osten*
110. Applied Microphotonics, *edited by Wes R. Jamroz, Roman Kruzelecky, and Emile I. Haddad*
111. Organic Light-Emitting Materials and Devices, *edited by Zhigang Li and Hong Meng*
112. Silicon Nanoelectronics, *edited by Shunri Oda and David Ferry*
113. Image Sensors and Signal Processor for Digital Still Cameras, *Junichi Nakamura*
114. Encyclopedic Handbook of Integrated Circuits, *edited by Kenichi Iga and Yasuo Kokubun*
115. Quantum Communications and Cryptography, *edited by Alexander V. Sergienko*
116. Optical Code Division Multiple Access: Fundamentals and Applications, *edited by Paul R. Prucnal*
117. Polymer Fiber Optics: Materials, Physics, and Applications, *Mark G. Kuzyk*
118. Smart Biosensor Technology, *edited by George K. Knopf and Amarjeet S. Bassi*
119. Solid-State Lasers and Applications, *edited by Alphan Sennaroglu*
120. Optical Waveguides: From Theory to Applied Technologies, *edited by Maria L. Calvo and Vasudevan Lakshiminarayanan*
121. Gas Lasers, *edited by Masamori Endo and Robert F. Walker*
122. Lens Design, Fourth Edition, *Milton Laikin*
123. Photonics: Principles and Practices, *Abdul Al-Azzawi*
124. Microwave Photonics, *edited by Chi H. Lee*
125. Physical Properties and Data of Optical Materials, *Moriaki Wakaki, Keiei Kudo, and Takehisa Shibuya*
126. Microlithography: Science and Technology, Second Edition, *edited by Kazuaki Suzuki and Bruce W. Smith*

MICROLITHOGRAPHY

Science and Technology

Second Edition

edited by
Kazuaki Suzuki
Bruce W. Smith

CRC Press
Taylor & Francis Group
Boca Raton London New York

CRC Press is an imprint of the
Taylor & Francis Group, an informa business

CRC Press
Taylor & Francis Group
6000 Broken Sound Parkway NW, Suite 300
Boca Raton, FL 33487-2742

Printed in the United States of America on acid-free paper
10 9 8 7 6 5 4 3 2 1

International Standard Book Number-10: 0-8247-9024-3 (Hardcover)
International Standard Book Number-13: 978-0-8247-9024-0 (Hardcover)

Library of Congress Cataloging-in-Publication Data

Microlithography : science and technology / editors, Kazuaki Suzuki and Bruce W. Smith. -- 2nd ed.
p. cm. -- (Optical science and engineering series)
"A CRC title."
Includes bibliographical references and index.
ISBN-13: 978-0-8247-9024-0 (alk. paper)
ISBN-10: 0-8247-9024-3 (alk. paper)
1. Microlithography--Industrial applications. 2. Integrated circuits--Masks. 3. Metal oxide semiconductors, Complementary--Design and construction. 4. Manufacturing processes. I. Suzuki, Kazuaki. II. Smith, Bruce W., 1959-

TK7836.M525 2007
621.3815'31--dc22 2006031516

Visit the Taylor & Francis Web site at
http://www.taylorandfrancis.com

and the CRC Press Web site at
http://www.crcpress.com

Preface

Over the last three decades, accomplishments in microlithographic technology have resulted in tremendous advances in the development of semiconductor integrated circuits (ICs) and microelectromechanical systems (MEMS). As a direct result, devices have become both faster and smaller, can handle an ever increasing amount of information, and are used in applications from the purely scientific to those of everyday life. With the shrinking of device patterns approaching the nanometer scale, the wavelength of the exposing radiation has been reduced from the blue-UV wavelength of the mercury *g*-line (436 nm) into the mercury *i*-line(365 nm), deep UV (DUV), vacuum UV (VUV), and the extreme UV (EUV). The krypton fluoride (KrF) excimer laser at 248 nm was adopted as an exposure source in DUV regions and has been used in volume manufacturing since 1988.

Since the first edition of this book, advances in 193-nm argon flouride (ArF) excimer laser lithography have allowed for the pursuit of sub-90-nm device fabrication and, when combined with high NA technology, polarized illumination, and immersion imaging, may be capable of imaging for device generations at 45 nm and beyond. The next generation of lithographic systems for 32-nm device technology will likely come from candidates including F_2 excimer laser (157 nm) lithography, EUV (13.5 nm) lithography, electron projection lithography (EPL), nanoimprint lithography (NIL), or maskless lithography (ML2). Among these candidates, ML2 such as electron-beam direct-write system has been used for small-volume device production with quick turn around time (QTAT) because a mask is not necessary. Factors that will determine the ultimate course for a high-volume device production will include cost, throughput, resolution, and extendibility to finer resolution.

The second edition of this volume is written not only as an introduction to the science and technology of microlithography, but also as a reference for those who with more experience so that they may obtain a wider knowledge and a deeper understanding of the field. The purpose of this update remains consistent with the first edition published in 1998 and edited by Dr. James R. Sheats and Dr. Bruce W. Smith. New advances in lithography have required that we update the coverage of microlithography systems and approaches, as well as resist materials, processes, and metrology techniques.

The contributors were organized and revision work started in 2003. Additional content and description have been added regarding immersion lithography, 157-nm lithography and EPL in Chapter 1 *System Overview of Optical Steppers and Scanners*, Chapter 3 *Optics for Photolithograph*, Chapter 5 *Excimer Laser for Advanced Microlithography*, and Chapter 6 *Electron Beam Lithography Systems*. Because the topics of EUV and imprint lithography were not addressed in the first edition, Chapter 8 and Chapter 9 have been added to discuss these as well. A detailed explanation of scatterometry has been incorporated into Chapter 14 *Critical Dimensional Metrology*. Chapter 15 *Electron Beam Nanolithography* has also has been widely revised. In order to maintain the continuity of this textbook, that proved so valuable in the first edition, these topics and others that may be less obvious, but no less significant, have been tied into the other corresponding chapters as necessary. As a result, we are certain that this second edition of *Microlithography: Science and Technology* will remain a valuable textbook for students, engineers, and researchers and will be a useful resource well into the future.

Kazuaki Suzuki
Bruce W. Smith

Editors

Kazuaki Suzuki is a project manager of Next Generation Lithography Tool Development at the Nikon Corporation. He has joined several projects of new concept exposure tools such as the first generation KrF excimer laser stepper, the first generation KrF excimer laser scanner, the electron-beam projection lithography system, and the full field EUV scanner. He has authored and coauthored many papers in the field of exposure tools and related technologies. He also holds numerous patents in the areas of projection lens control systems, dosage control systems, focusing control systems, and evaluation methods for image quality. For the last several years, he has been a member of program committees such as SPIE Microlithography and other international conferences. He is an associate editor of The Journal of Micro/Nanolithography, MEMS, and MOEMS (JM3). Kazuaki Suzuki received his BS degree in plasma physics (1981), and his MS degree in x-ray astronomy (1983) from Tokyo University, Japan. He retired from a doctorate course in x-ray astronomy and joined the Nikon Corporation in 1984.

Bruce W. Smith is a professor of microelectronic engineering and the director of the Center for Nanolithography Research at the Rochester Institute of Technology. He is involved in research in the fields of DUV and VUV lithography, photoresist materials, resolution enhancement technology, aberration theory, optical thin film materials, illumination design, immersion lithography, and evanescent wave imaging. He has authored numerous scientific publications and holds several patents. Dr. Smith is a widely known educator in the field of optical microlithography. He received his MS degree and doctorate in imaging science from the Rochester Institute of Technology. He is a member of the International Society for Photo-optical Instrumentation Engineering (SPIE), the Optical Society of America (OSA), and the Institute of Electrical and Electronics Engineers (IEEE).

Contributors

Mike Adel KLA-Tencor, Israel

Robert D. Allen IBM Almaden Research Center, San Jose, California

Zvonimir Z. Bandić Hitachi San Jose Research Center, San Jose, California

Palash Das Cymer, Inc., San Diego, California

Elizabeth A. Dobisz Hitachi San Jose Research Center, San Jose, California

Gregg M. Gallatin IBM Thomas J. Watson Research Center, Yorktown Heights, New York (Current Affiliation: Applied Math Solutions, LLC, Newton, Connecticut)

Charles Gwyn Intel Corporation (Retired)

Maureen Hanratty Texas Instruments, Dallas, Texas

Michael S. Hibbs IBM Microelectronic Division, Essex Junction, Vermont

Roderick R. Kunz Massachusetts Institute of Technology, Lexington, Massachusetts

Gian Lorusso IMEC, Leuven, Belgium

Chris A. Mack KLA-Tencor FINLE Divison, Austin, Texas (Retired, Currently Gentleman Scientist)

Herschel M. Marchman KLA-Tencor, San Jose, California (Current Affiliation: Howard Hughes Medical Institute, Ashburn, Virginia)

Martin C. Peckerar University of Maryland, College Park, Maryland

Douglas J. Resnick Motorola, Tempe, Arizona (Current Affiliation: Molecular Imprints, Austin, Texas)

Bruce W. Smith Rochester Institute of Technology, Rochester, New York

Kazuaki Suzuki Nikon Corporation, Saitama, Japan

Takumi Ueno Hitachi Chemical Electronic Materials R&D Center, Ibaraki, Japan

Stefan Wurm International SEMATECH (Qimonda assignee), Austin, Texas

Sanjay Yedur Timbre Technologies Inc., a division of Tokyo Electron Limited, Santa Clara, California

Contents

Part III Metrology and Nanolithography

11

Resist Processing

Bruce W. Smith

CONTENTS

11.1 Introduction

For the most part, conventional single-layer photoresists have been based on components with two primary functions. Whether considering older bis(arylazide)-*cis*-polyisoprene resists, diazonapthoquinone (DNQ)/novolac *g*/*i*-line resists, or chemically amplified polyhydroxystyrene (PHOST) or polymethacrylates, deep-UV (DUV) resists, an approach has been utilized wherein a base resin material is modified for sensitivity to exposure by a photoactive compound or through phtotoinduced chemical amplification. The resist base resin is photopolymeric in nature and is responsible for etch resistance, adhesion, coatability, and bulk resolution performance. These resins generally do not exhibit photosensitivity on the order required for integrated circuit (IC) manufacturing. Single-component polymeric resists have been utilized for microlithography, including methacrylates, styrenes, and other polymers or copolymers, but sensitization is generally low and limited to exposures at short ultraviolet (UV) wavelengths or with ionizing radiation. Inherent problems associated with low absorbance and poor radiation resistance (required, for example, during ion implantation or plasma etching steps) generally limit the application of these types of resists to low volumes or processes with unique requirements.

Sensitization of photoresist materials has been accomplished by several methods. In the case of conventional *g*/*i*-line resists, a chemical modification of a base-insoluble photoactive compound (PAC), the diazonaphthoquinone, to a base-insoluble photoproduct, indene carboxylic acid (ICA), allows an increase in aqueous base solubility. For chemically amplified resists, exposure of a photoacid generator (PAG) leads to the production of an acid, which subsequently allows polymer deprotection (positive behavior) or cross-linking (negative behavior). Other similar processes have been developed (as discussed in Chapter 10) and may involve additional components or mechanisms.

For any resist system, the thermodynamic properties of polymeric resins play an important role in processability. During the coating, exposure, and development processes of a resist, an understanding of the thermodynamic properties is desirable because the glass transition temperature (T_g) of a polymer influences planarizability, flow, and diffusion, Although reasonably high T_g values may be desirable, glassy materials with values above 200°C are not suitable because of poor mechanical performance. After three-dimensional resist features are formed, however, a thermoset material may be desired in which the polymer does not flow with temperature and a T_g essentially does not exist. This ensures the retention of high-aspect-ratio features through subsequent high-temperature and high-energy processes. By appropriate engineering of back steps during single-layer resist processing, the control of polymer thermoplastic and thermoset properties can be made possible. For negative resists, the situation is inherently simplified. Coated negative resists are thermoplastic in nature, with a well-defined T_g range. Upon exposure and subsequent secondary reactions, cross-linking leads to a networked polymer that will not flow with temperature. At the temperature of decomposition (T_d) the polymer will break down and begin to

lose significant volume. Imaging steps are therefore responsible for the production of thermally stable resist features. Operations are often included in the processing of positive resists that can accomplish similar thermal stability enhancements.

This chapter addresses the critical issues involved in the processing of single-layer resists materials. Process steps to be discussed include:

- Resist stability, contamination, and filtration
- Substrate priming
- Resist coast
- Soft bake
- Exposure
- Postexposure brake
- Development
- Swing effects
- Hard bake and postdevelopment treatment

The step-by-step process flow for DNQ/novolac resists has been covered elsewhere, and the reader is directed to these references for additional description [1–3]. Specific details are given here for positive DNQ/novolac resists and both positive and negative DUV chemically amplified resists based.

11.2 Resist Stability, Contamination, and Filtration

11.2.1 DNQ/Novolac Resist Stability and Filtration

DNQ/novolac resists have proved to be robust materials with respect to sensitivity to thermodynamic and aging effects while stored in uncast form. A resist shelf life of several months can be expected with no significant change in lithographic performance. Because resists are considered for application in production, the stability of materials at various points of the process also needs to be considered.

For DNQ/novolac resists, aging can lead to an increase in absorption at longer wavelengths. Resists materials are susceptible to several thermal and acid/base (hydrolytic) reactions when stored [4]. These include thermal degradation of the DNQ to ICA followed by acid-induced azo dye formation and an azo coupling of the DNQ and novolac. A characteristic "red darkening" results from this coupling, induced by the presence of acids and bases in the resist. Although long-wavelength absorbance is altered by this red azo dye, the impact on UV absorbance and process performance is most often negligible. Degradation mechanisms can also result in cross-linking, leading to an increase in high-molecular-weight components. Hydrolysis of DNQ may occur to form more soluble products and hydrolysis of solvents is possible, which can lead to the formation of acids [5]. The practical imitation of shelf life for DNQ/novolac resists is generally on the order of 6 months to 1 year. Once coated, resist film can absorb water and exhibit a decrease in sensitivity, which can often be regained through use of a second soft bake step. As will be described, process delays for chemically amplified PHS resists are much more critical than for DNQ/novolac materials.

A larger problem encountered when storing DNQ/novolac resists is sensitizer precipitation. With time, DNQ PAC can fall out of solution, especially at high temperatures.

These crystallized precipitates most readily form with high levels of DNQ. In addition, resist particulate levels can be increased by the formation of gel particles, a result of acid-induced novolac cross-linking via thermal decomposition of DNQ. Any of these routes to particulate formation can lead to levels exceeding that measured by the resist manufacturer. Because of this, point-of-use filtration has become common practice for most production applications to ensure photoresist consistency [6]. Resist materials are commonly filtered at a level of approximately 25% of the minimum geometry size. As the geometry size approaches sub −0.35 μm, filtration requirements approach 0.05 μm. Such ultrafiltering will have an impact on how resist can the manufactured and used. Filtration speed is dramatically reduced and material preparation become more costly. Similar concerns can exist for pump through put during resist dispensing. Fractionation of a resist material can also occur, resulting in the removal of long polymer chains and a change in process performance. To illustrate this, consider an *i*-line (DNQ/novolac) with a molecular weight on the order of 1020×10^3 g/mol (number average). The resulting average polymer chain size is nearly 5–6 nm with a maximum as large as 40 nm. In highly concentrated resist formulations (greater than 30 wt.%), intertwisting of polymers can result in chain sizes greater than 80 nm. If such a resist is filtered to 0.05 μm, the largest polymer chains can be removed. As technology progresses toward smaller feature resolution, it is clear that particulate and filtration issues need to be carefully considered.

11.2.2 Stability Issues for Chemically Amplified PHOST Resists

Filtration concerns for *i*-line resists are extended to deep-UV lithography when PHS resists are considered. As sub−0.2-μm geometry is pursued, the issue of ultrafiltering becomes an increasingly important problem. In addition, environmental stability issues are present for many chemically amplified resists (CARs) that are not issues for DNQ/novolac resists, especially for resists based on acid-catalyzed reactions and PHOST resins. Ion-exchange methods are conventionally used to reduce ion contamination levels in resists below 50 ppb. Ionic contamination reduction in both positive and negative CAR systems needs to be carefully considered. Deprotection of acid-labile components can result from reaction with cationic exchange resins. The catalytic acid produced upon exposure of these resists is also easily neutralized with base contamination at ppb levels. These contaminants can include such things as ammonia, amines, and NMP, which are often present in IC processing environments [7]. Any delay between exposure and postexposure bake (PEB) can result in a decrease in sensitivity and the formation of a less-soluble resist top layer or "T-top."

To reduce the likelihood of base contamination of these resists, several improvements have been made in resist formulations. One method to reduce acid loss is the use of low-activation-energy (E_a) polymers with highly reactive protection groups. These resists are sufficiently active that deprotection can occur immediately upon exposure, significantly reducing the sensitivity to PEB delay effects [8,9]. Additives have also been incorporated into DUV PHOST resists to improve their robustness to contamination effects [10,11] and resist top-coating approaches have been introduced [12]. By coating a thin water-soluble transparent polymeric film over a resist layer, protection from airborne contamination can be made possible. This "sealing" layer is removed prior to development with a water rinse. Although such a solution leads to minimal additional process complexity, it is still desirable to use resist techniques that do not require additional material lavers. An alternative route for the reduction of contamination effect is the use of high-activation-energy resist materials. By reducing the reactivity of a resist, higher bake-process temperatures are allowed. Increasing the bake temperatures above a polymer's T_g results in a

densification of the photoresist. This leads to a significant decrease in the diffusion rate of airborne base contamination prior to or after exposure [13,14]. These high-E_a resists also require that a photoacid generator be chosen that can withstand high temperatures. Other methods used to reduce base contamination of acid-catalyzed resists include the use of activated charcoal air filtration during resist coating exposure, and development operations [15]. This is now considered a requirement for processing of PHOST CAR resists. Environmental base contamination can be neutralized and further reduced by adding weak acids to these filters.

The stability or shelf life of PHOST-based resists is also influenced by the structure of polymer protective groups. This is especially true for low-activation-energy (high-reactivity) resists, for which the lability of protective groups may decrease usable resist life. Conversely, the more stale protective groups utilized with high-activation-energy (low-reactivity) resists lead to a higher degree of stability.

11.3 Resist Adhesion and Substrate Priming

Adequate adhesion of photoresist to a wafer surface is critical for proper process performance. Resist adhesion failure can occur not only during photolithography operations, but also in subsequent etch, implant, or other masking steps. Negative resists are less prone to adhesion failure because as cross-linking results in a networked polymer that is bound to the wafer surface. Positive resists (especially phenolic-based materials such as novolac or PHOST resists) are more likely to be single-polymer chains and rely on weaker physical and chemical forces for adhesion. Etch-process undercutting can often result from inadequacies at the resist interface, resulting in loss of etch linewidth control. The causees of resist adhesion failure are generally related to dewetting of a photoresist film. This can result from a large discordance between the surface tension of the wafer and that of the resist material, especially when coating over silicon oxide. Silicon dioxide is an especially difficult layer to coat because it provides a hydrophilic (water attracting) surface to a hydrophobic (water repelling) resist. The surface tension of thermal silicon dioxide may be on the order of 15 dynes/cm^2, whereas the surface tension of phenolic resists in casting solvent may be near 30 dynes/cm^2. Surface defects can also cause adhesion failure as surface free energy can result in dewetting.

Methods of adhesion promotion can be used for most silicon oxide layers, whether they are thermally grown, deposited, native, or glasslike. Chemical passivation of these surfaces is generally carried out using silylating priming agents that act to modify the wafer surface. Some benefit can be realized with priming of layers other than oxides if techniques promote a closer matching of material surface tension. Alkylsilane compounds are generally used to prime oxide surfaces, leading to a lowering of surface hydrophilicity. The most commonly used silane-type adhesion promoter is hexamethyldisilazane (HMDS). Other similar promoters are available, including trimethylsilyldiethylamine (TMSDEA), which can be more effective but also less stable, resulting in lower shelf and coated lifetimes. Reduction of substrate surface tension is carried out in two stages, as shown in Figure 11.1. The figure depicts a silicon oxide surface with adsorbed water and OH^- groups. An initial reaction of water with an alkylsilane (HMDS) produces an inert hexamethyldisiloxane and ammonia, resulting in a dehydrated surface. Further reaction with HMDS produces a trimethylsilyl-substitued hydroxyl or oxide species and unstable trimethylsilylamine. With heat, this unstable compound reacts with

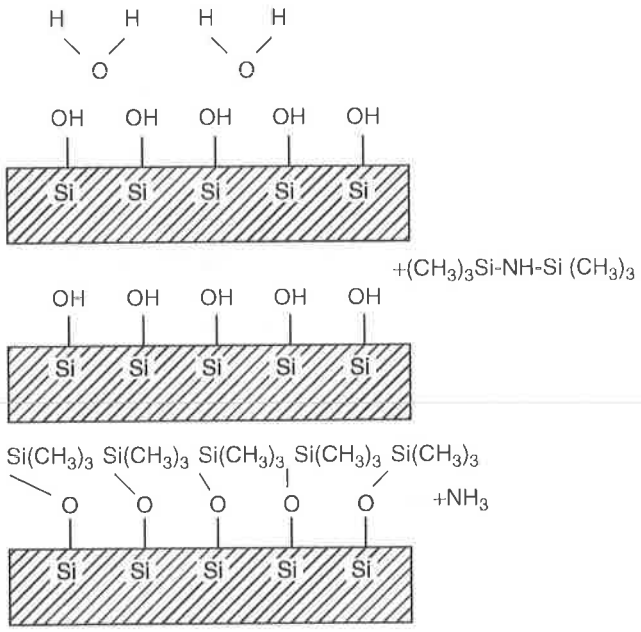

FIGURE 11.1
Adhesion promotion of a silicon oxide surface with HMDS surface priming. The substrate is first dehydrated upon reaction with silane promoter. Further reaction with heat leads to a hydrophobic surface.

other surface hydroxyl groups to produce further ammonia and a trimethylsiloxy species. The process continues until steric hindrance (via the large trimethylsilyl groups) inhibits further reaction.

Surface priming using HMDS, TMSDEA, or similar agents can be carried out in either liquid- or vapor-phase modes. In either case, elevated process temperatures (~100°C) must be reached to complete the priming reaction. Substrates should be cleaned prior to application using UV ozone, HF dip, plasma, or other "oxidative" cleaning methods. Adhesion of a photoresist to silicon nitride or deposited oxide layers can be enhanced by using an oxygen/ozone plasma treatment. Priming agents are generally best applied using vapor prime methods in either line or in batch vacuum ovens. Uniformity and reduced chemical usage make this more attractive than liquid methods.

Overpriming of a wafer surface can result in dewetting and lead to further adhesion problems. This can occur with repeated treatment or by using excessive vapor times. Problems are often noticed in isolated substance areas, depending on device topography or condition. A phenomenon known as resist "popping" can also occur as a result of overpriming; in this case, high-fluence exposure (such as that encountered with heavy UV overexposure in ion implantation steps) can cause failure of weakened resist adhesion. Deposition of resist debris onto adjacent substrate areas can result. Measurements of resist surface tension using water contact angle techniques can identify such overpriming problems. Remedies include the use of shorter priming times, resist solvents with lower surface tension, double resist coating steps, or a pretreatment of the wafer surface with the resist casting solvent. Oxygen or ozone plasma treatments can also correct an overprimed wafer surface and allow repriming under more appropriate conditions.

The strength of adhesion bonds between a photoresist and a substrate has also been shown to influence the T_g and thermal expansion coefficient of a thin film. The impact is greatest as resist films approach 1000-Å thicknesses [16].

11.4 Resist Coating

11.4.1 Resist Spin-Coating Techniques and Control

A photoresist can be dispensed by several methods, including spin coating, spray coating, and dip coating. The most widely used method for coating resists onto wafer substrates are spin coating methods. During spin coating, the resist is dispensed onto a wafer substrate (either statically or dynamically), accelerated to final spin speed, and cast to a desired film thickness. Variations on this process have been suggested, including the use of a short-term high-speed initial coating step followed by a slow drying stage [17]. Spin-coating processes use the dynamics of centrifugal force to disperse a polymeric resist material over the entire wafer surface. The flow properties (rheology) of the resist influence the coating process and need to be considered to achieve adequate results [18]. In addition, solvent transport through evaporation occurs, which can result in an increase in resist viscosity and shear thinning, both of which affect the final film properties. As a resist-solvent material is spin cast, the film thickness decreases uniformly at a rate dependant on the spin speed (ω), kinematic viscosity (v), solids concentration (c), solvent evaporation rate (e), and initial film thickness, expressed by the following rate equations:

$$\frac{dS}{dt} = \frac{-c2\omega^2 h^3}{3v}, \tag{11.1}$$

$$\frac{dL}{dt} = (1-c)\frac{2\omega^2 h^3}{3v} - e, \tag{11.2}$$

where dS/dt and dL/dt are rate of change of solids (S) and solvents (L), respectively [19]. The results are shown in Figure 11.2 for a 1-μm film, where both solids and solvent volumes are plotted against spin time. Initially, concentration changes little as resist spread dominates. When the resist thickness drops to one-third of its original value, evaporation dominates and solvent content reaches its final value. The high viscosity of the resist eliminates further flow.

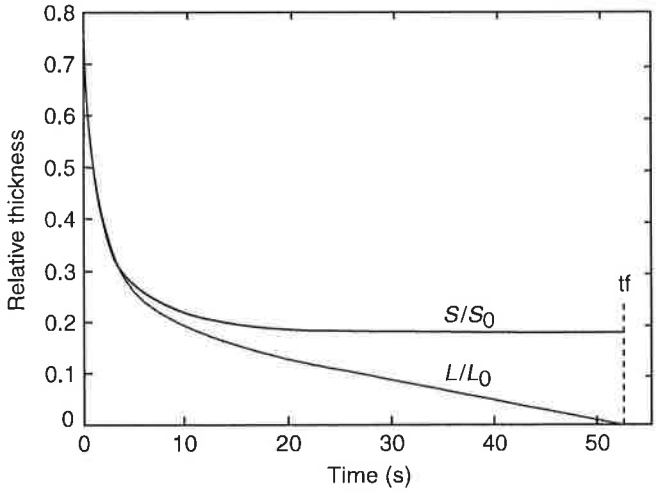

FIGURE 11.2
Calculated time dependance during spin coating on the volume of solids (S) and solvent (L) per unit area normalized to initial values. When the resist thickness drops to one third of its original value, evaporation dominates and the solvent content reaches its final value. (From Meyerhofer, D., *J. Appl. phys.*, 49(7), 3993, 1978.)

The primary material factors that influence spin-coated film properties include the resist polymer molecular weight, solution viscosity, and solvent boiling point (or vapor pressure). Primary process factors include wafer spin speed, acceleration, temperature, and ambient atmosphere. The thickness of a resist film can be modified to some extent through control of the rotation speed of the substrate. Resist thickness in inversely proportional to the square root of spin speed (ω):

$$\text{Thickness} \propto \frac{1}{\sqrt{\omega}}. \tag{11.3}$$

To achieve large thickness changes, modification of the resist solution viscosity is generally required because coating at excessively low or high speeds results in poor coating uniformity. At excessively high speeds, mechanical vibration and air turbulence result in high levels of across-wafer nonuniformity. At low spin speeds, solvent loss of the resist front as it is cast over the substrate results in a situation of dynamic resist viscosity, also resulting in high levels of nonuniformity. The optimal spin range is dependent on wafer size. Wafers up to 150 mm can be coated at rotation speeds on the order of 4000–5000 rpm. Larger substrates require lower speeds.

The optimum coating thickness for a resist layer is determined by the position of coherent interference nodes within the resist layer. Standing waves (see Section 11.9) resulting from reflections at the resist/substrate interface result in a regular distribution of intensity from the top of the resist to the bottom. This distribution results in a "swing" in the required clearing dose (E_0) for a resist, as shown in Figure 11.3. Three curves are shown, for polysilicon, silicon nitride (1260 Å), and silicon dioxide (3700 Å) coated substrates. A general upward tend in E_0 is seen as resist thickness increases. This is due to the residual nonbleachable absorption of the resist, which can be significant. (For a resist with a residual absorption of 0.10 μm^{-1}, the intensity at the bottom of a 1-μm resist layer is 90% of that experienced at the top.) In addition to this E_0 trend, sensitivity oscillates from minimum to maximum values with thickness. Within one swing cycle, an exposure variation of 32% exists for the polysilicon substrate, 27% for silicon nitride, and 36% for silicon

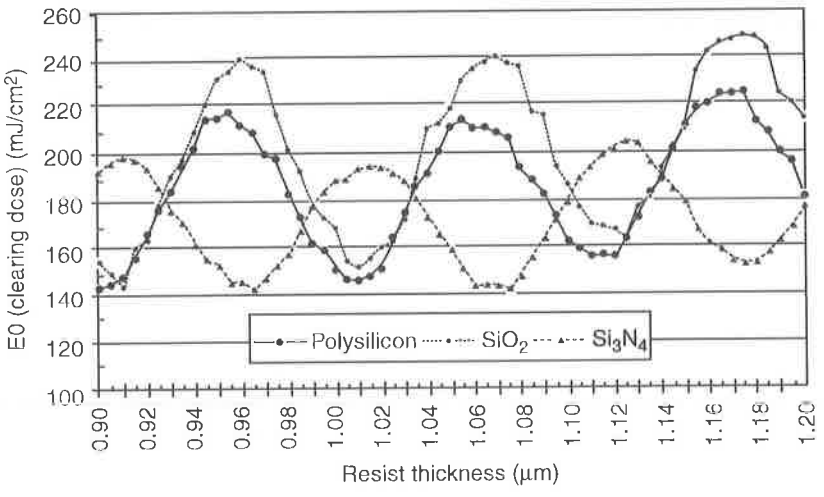

FIGURE 11.3
Clearing dose (E_0) swing curves for an *i*-line resist over polysilicon, silicon dioxide (3700 Å), and silicon nitride (1260 Å). The increasing trend in required dose is a function of residual absorption. Conditions of minimum interference leads to maximum E_0 values but minimal scumming.

dioxide. When a resist is coated over a dielectric layer, such as silicon dioxide, silicon nitride, or an antireflective coating (ARC), there will be a shift in the phase of E_0 oscillations. Analysis of swing behavior may therefore be unique for various lithographic levels. Coated thickness optimization can be performed using these swing curves, determined experimentally through open frame exposure of a resist coated within a small range of thicknesses. Lithographic modeling can aid in the generation of such relationships using knowledge of the resist refractive index, absorption properties (possibly dynamic), exposure wavelength, and resist/substrate reflectivity.

Inspection of the E_0 swing curve in Figure 11.3 suggests several possibilities for resist thickness, of which only a few are desirable. For polysilicon, there is a minimum dose requirement at a thickness of $\sim$1.01 μm, where constructive interference occurs, and there is maximum intensity at the resist base. At a resist thickness over polysilicon of $\sim$1.06 μm, destructive interference leads to a maximum E_0 requirement. Other alternatives might include positions on either side of these values (between nodes). Thicknesses corresponding to these midnodal positions allow the least amount of coating process latitude, as small deviations from the targeted film thickness lead to significant changes in dose requirements. Greater latitude exists at maximum interference positions, where there is a minimum requirement for exposure dose, which may be an attractive choice. Small changes in film thickness result only in small E_0 variations, but the direction of these changes is toward higher clearing dose values. The result may be scumming of resist features resulting from underexposure, a situation that is unacceptable. The best choice for targeted film thickness may be at a corresponding interference minimum, where small thickness changes result in a small decrease in the dose requirement. Slightly lower throughput may result (generally not a gating factor in today's exposure operations) but this will ensure no resist scumming related to underexposure. Image fidelity at the top surface of a resist film is also influenced by film thickness and positions on the interference curve. By coating at a midnodal thickness, top surface rounding, or T-topping can result (see the Section 11.9 for further discussion).

During spin coating, a large amount of resist "free volume" can be trapped within a resist layer. A simplified free-volume model of molecular transport can be quite useful for correlation and prediction of diffusion properties of resist materials [20,21]. (The reader is directed to Refs. 20 and 21 for a detailed discussion of diffusion in polymer-solvent systems.) Volumetric expansion enhances polymer chain mobility and acts similarly to the addition of plasticizers. The resist's glass transition temperature (T_g) is lowered and the dissolution properties of novolac- and PHOST-based resist can be increased [22]. Coating-included free volume has been shown to affect acid diffusion as well and becomes a concern when considering reduction of airborne base contamination and post-exposure delay.

11.4.2 Solvent Contribution of Film Properties

Residual casting solvent can act as a plasticizer and can reduce the T_g of a resist. Resist solvent content has been shown to be dependent on film thickness. A 1000-Å resist film may, for example, exhibit 50% more solvent retention than a 10,000-Å film. Figure 11.4 shows residual solvent in PHOST polymer films coated at thicknesses of 12,000 and 1100 Å. Only near the resist T_g (135°C) does the solvent content for the 1100-Å film approach that of the thicker film. Table 11.1 shows diffusion coefficients for PGMEA solvent in the same PHOST film thicknesses, determined by diffusion analysis during 2 h of baking. These results may be due to a smaller degree of inter- or intramolelcular hydrogen bonding in thinner films [23–25], which can allow a stronger polymer

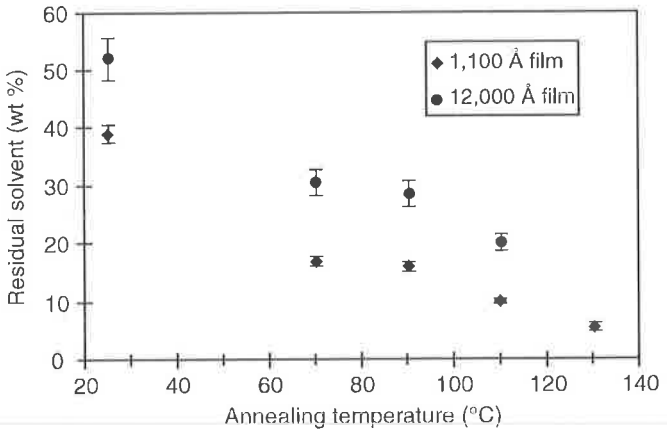

FIGURE 11.4
Back-temperature dependence of residual PGMEA solvent in 1100-Å and 12,000-Å spin-cast films annealed for 1300 min. (From Frank, C.W., Rao, V., Despotopoulou, M.M., Pease, R.F.W., Hinsberg, W.D., Miller, R.D., and Robolt, R.F., *Science*, 273, 972, 1996.)

interaction with the casting solvent and lower solvent evaporation rates. A higher solvent content leads to an increased dissolution rate and increased diffusivity levels. When considering various resist solvent systems, it might also be expected that lower boiling point (T_b) solvents would lead to lower solvent retention than higher T_b solvents. The opposite, however, has been demonstrated [26]. PGMEA, for instance, has a boiling point of 146°C and an evaporation rate of 0.34 (relative to *n*-butyl acetate). Ethyl lactate has a higher T_b of 154°C and an evaporation rate of 0.29. Despite its lower boiling point, PGMEA is more likely to be retained in a resist film. The reason for this is a skin formation that results from rapid solvent loss during the coating process [27]. The resist viscosity at the surface increases more rapidly for PGMEA as solvent is exhausted, leading to more residual solvent remaining throughout the resist film. If a resist film is then baked at temperatures below the bulk T_g, densification of surface free volume is allowed only at the top surface of the film and is prevented throughout the bulk. Entrapped solvent therefore leads to an apparent surface-induction effect, which can be reduced only if the resist is backed above its T_g. Because solvent content plays an important role in determining the ultimate glass transition temperature of the resist (and therefore its dissolution properties), any postcoating incorporation of solvents can also have an adverse impact on performance. Such additional solvent may be encountered, for instance, when using an edge bead removal process based on acetone, ethyl lactate, pentanone, or other organic solvents.

11.4.3 Substrate Contribution to Resist Contamination

Continuous improvements have been made in the materials and processes used for DUV PHS chemically amplified resists to reduce top-surface base contamination effects.

TABLE 11.1
Diffusion Coefficients of PGMEA Solvent in PHS Films from 2 h of Baking

	Diffusion Coefficient (cm^2/s)	
Temperature (°C)	**0.11-μm Film**	**1.2-μm Film**
70	4.2×10^{-14}	1.2×10^{-12}
90	9.4×10^{-14}	4.4×10^{-12}
110	1.1×10^{-13}	1.4×10^{-11}

An additional contamination problem occurs when processing PHS resists over some substrates. Resists coated over Si_3N_4, boro-phospho-silicate glass (BPSG), spin-on-glass (SOG), Al, and TiN have seen shown to initiate a substrate contamination effect that can result in resist scumming or "footing." With TiN substrates, the problem has been attributed to surface N^{-3} and TiO_2, which can act to neutralize photogenerated acid, resulting in a lowering of the dissolution rate at the resist/substrate interface [28]. Sulfuric acid/hydrogen peroxide and oxygen plasma pretreatments have been shown to reduce contamination effects when coating over Si_3N_4 and other problematic substrates [29].

11.4.4 Edge-Bead Removal

After a spin-coating process, a bead of hardened resist exists at the edge of a wafer substrate. Formation of this edge bead is caused in part by excessive resist drying and can result in resist accumulation up to 10 times the thickness of the coated film. Elimination of this edge bead is required to reduce contamination of process and exposure tools. Solvent edge-bead removal (EBR) techniques can be utilized to remove this unwanted resist by spraying a resist solvent on the backside and/or the frontside of the wafer substrate. Surface tension allows removal of a 2–3-mm resist edge from the front resist surface while removing any backside resist coating. Acetone, ethyl lactate, and pentanone are possible solvent choices for edge-bead removal processes.

11.5 Resist Baking—Soft Bake

11.5.1 Goals of Resist Baking

Baking processes are used to accomplish several functions and generally alter the chemical and/or physical nature of a resist material. Goals of resist baking operations may include the following that are accomplished at various stages during resist processing:

- Solvent removal
- Stress reduction
- Planarization
- Reduction of resist voids
- Reductions of standing waves
- Polymer crosslinking and oxidation
- Polymer densification
- Volatilization of sensitizer, developer, and water
- Induction of (acid) catalytic reactions
- Sensitizer/polymer interactions

Polymeric resist resins are thermoplastic in nature, more amorphous than crystalline, and have glass transition temperatures in the 70°C–180°C range. Thermal flow properties are taken advantage of during processing, in which baking steps at or near the T_g allow some degree of fluid-like resist behavior. In a fluid-like state, stress in a coated film can be reduced and diffusion of solvents, sensitizer, and photoproducts is enhanced. At high resist baking temperatures, sensitizer and polymer decomposition can occur. A proper

choice of the baking temperature, time, and method must therefore take into account the evaporation and diffusion properties of solvents, decomposition temperature of PAC or PAG, and diffusion properties of the photoinduced acid and base contaminants for chemically amplified resist material.

11.5.2 Resist Solvent and T_g Considerations

There is a relationship between a solvent's evaporation rate or boiling point and the residual solvent content in a resist film. Obtaining such a relationship is difficult, however, because residual solvent is highly dependent on the T_g of the resist. If a baking process does not sufficiently reach the resist T_g, it is difficult to remove solvent to levels below a few percent [30]. The resist T_g therefore plays an important role in the evaporation mechanisms of resist solvent removal. Solvent removal has been shown to occur in two stages: the first stage is the diffusion of solvent molecules at temperatures near T_g and their accumulation at the film surface. The second stage is the evaporation of these adsorbed molecules at higher temperatures, dependent on hydrogen bonding properties.

No compaction would be expected if baking temperatures above the resist bulk T_g values were not reached. In fact, soft bake temperatures 10°C–20°C below a bulk resist T_g are frequently employed with successful results. The reason for this is that the T_g of a resist film is not identical to that of bulk resist. It may actually be a great deal lower. This can be explained by the concept of resist free volume, which is minimized if soft bake temperatures above the bulk T_g values are used. If resists are baked more than 5°C–10°C below the actual resist film T_g, compaction of this intrinsic free volume generally cannot occur [31].

Several resist material factors affect coated PHOST film flow properties and may be modified for optimum CAR performance. In general:

- Blocking of phenolic groups in PHOST generally results in a lowering of T_g, a consequence of the decrease in hydrogen bonding between phenolic groups.
- A 40°C–50°C decrease in polymer flow temperature (T_f) has been reported with 25% blocking of PHS [32].
- By modifying the molecular weight of the PHS polymer, 20°–25° of the loss in T_g or T_f due to blocking can be regained.
- As the number of phenolic groups is increased (relative to *t*-BOC protective groups), the deprotection temperature is reduced.
- As the number of the phenolic group is increased, T_g is also increased.

These relationships can result is a difficult situation if the deprotection temperature is forced lower than the resist T_g. Further manipulation may be possible through the use of copolymerization or by introducing additional hydrogen bonding sites.

There is a trade-off in determining the optimal soft bake temperature. A high soft bake temperature is desired so that the resist film T_g approaches that of the bulk, which leads to the best thermal performance. But at lower soft bake temperatures, an increase in post-exposure acid diffusion is made possible, allowing a reduction in standing waves. To accommodate a lower soft bake temperature, a higher postexposure bake (PEB) may be needed to achieve adequate thermal and plasma etch performance properties (see Section 11.7 for an additional description).

11.5.3 Soft Bake

Resist films are coated from a polymer solution, making solvent reduction of a coated film a primary action of soft bake (or prebake) processes. Other consequences of soft baking include a reduction of free volume and polymer relaxation, which have been suggested to be important phenomena that resist process performance [33]. Prior to coating, photoresist contains between 65 and 855 solvents. Once cast, the solvent content is reduced to 10%–20% and the film can still be considered in a "liquid" state. If it was exposed and processed at this point, several adverse consequences would result. At this high solvent level, the film is tacky and highly susceptible to particulate contamination, which can be transferred through handling to subsequent steps. Also, inherent stress resulting from casting a thin film leads to adhesion problems. The most significant impact resulting from the elimination of a soft bake step is lack of dissolution discrimination between exposed and unexposed resist. With such high solvent levels, the expanded resist volume allows a high degree of dissolution regardless of the state of inhibition, protection, acceleration, crosslinking. Ideally, a solvent content of a few percent would be desirable. Further densification could then be allowed to control the small molecular diffusion properties. To achieve this, the baking operation must approach the boiling point of the casting solvent (on the order of 140°C for conventional solvent systems). At this elevated temperature, decomposition of the resist sensitizer is likely to occur since DNQ decomposition temperatures are on the order of 100°C–120°C. Some residual solvent may also be desirable for DNQ/novolac to allow water diffusion and conversion of ketene to ICA. Complete solvent removal at prebake is therefore not attempted; instead, adequate removal to allow the best exposure and dissolution properties is targeted. Figure 11.5 shows the development rate vs. soft bake temperature for a DNQ/novolac resist. Four zones exist: (I) a no-bake zone where residual solvent and dissolution rates are high; (II) a low-temperature zone (up to 80°C) where the dissolution rate is reduced due to solvent removal; (III) a midtemperature zone (80°C–110°C) where DNQ is thermally converted to ICA, leading to an increase in development rate; and (IV) a high-temperature zone (greater than 120°C) where film densification occurs, DNQ is further decomposed, and water is removed, leading to an increase in inhibition rather

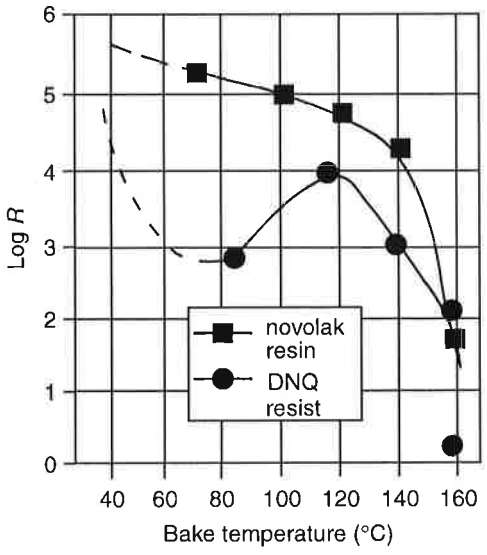

FIGURE 11.5
The influence of prebake temperature on dissolution rate (Å/min) for a novolac resin and a DNQ/novolac resist. Prebake time is 30 min, developer is 0.25 N KOH. (From Koshiba, M., Murata, M., Matsui, M., and Harita, Y., *Proc. SPIE*, 920, 364, 1998.)

than acceleration. Also, at these temperatures, oxidation and cross-linking of the novolac begin [34].

Whereas a prebake for DNQ/novolac is required to bring the resist to a state suitable for subsequent exposure and development, control to $\pm 1°C$ is generally adequate to ensure consistent lithographic performance. This is not the case for chemically amplified resists based on PHS, however. Because acid diffusion is an integral part of both positive and negative acid-catalyzed resist, control of polymer composition and density is critical. Consideration for soft bake differs for high-, and low-E_a CAR resists, depending on the reactivity of the resist to acid-induced deprotection. Resists with a moderate activation energy (E_a) had been the conventional route to positive CAR resists. By making use of resists with lower reactivity (high E_a), elevated baking processes above the polymer T_g (~150°C) allow maximum densification and reduction of the diffusion of acid-neutralizing contaminants. This resist design concept also reduces acid diffusion, which can result in an increase in resolution capability [35].

11.5.4 Resist Baking Methods

The preferred method of resist bake for IC applications utilizes conduction on a vacuum hot plate, usually in line with the entire resist process. Convection baking is another option, performed in an oven and generally used in a batch mode. Loading effects, slow recovery, and poor air circulation uniformity present problems for convection baking with current resist process demands. Microwave and infrared (IR) baking methods have been utilized to a limited extent, but the practicality of these methods is limited because of substrate incompatibility and process control. Both temperature and uniformity control are important for baking processes, the latter becoming most critical as chemically amplified resist requirements are considered. To achieve uniformity, careful consideration of the vacuum plate baking mechanics is required, including temperature uniformity, airflow, and cycle time. To meet the high demands of wafer-to-plate contact across an

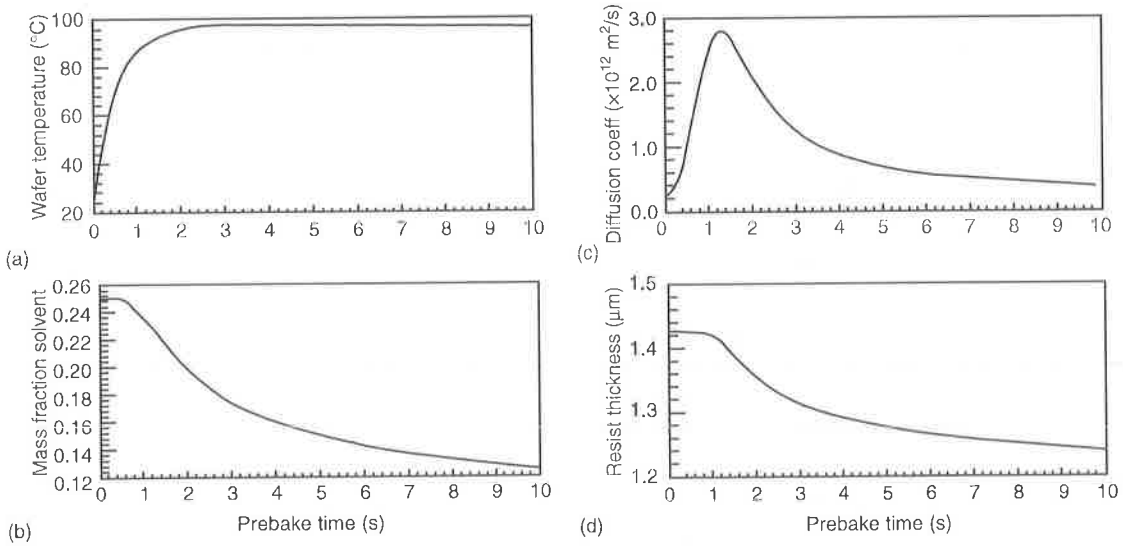

FIGURE 11.6
Mechanisms involved during the first ten seconds of hot plate baking of a resist. (a) Rise in wafer temperature; (b) solvent loss; (c) diffusivity; and (d) typical thickness change. (From Mack, C. A. et al., *Proc. SPIE*, 2195, 584, 1984.)

entire wafer, strict requirements are also placed on contamination control and resist edge-bead removal.

Figure 11.6 shows the mechanisms involved during the first 10 s of baking on a vacuum hot plate. Figure 11.6a shows that the temperature of the wafer increases with a rapid rise during the first seconds of baking and levels off after 3 s. Figure 11.6b illustrates the solvent loss during this time, which continues to decrease well out to 10 s and beyond. Figure 11.6c shows the shows the impact of baking time on diffusivity, which rises during the initial few seconds and then decreases. Figure 11.6d shows a typical change in resist thickness during baking, which decreases as the resist density increases.

11.6 Photoresist Exposure

11.6.1 Resist Exposure Requirements

Exposure of a photoresist involves the absorption of radiation and subsequent photochemical change, generally resulting in a modification of dissolution properties. The absorption characteristics of a photoresist largely influence its resolution and process capabilities. Resists based only on exponential attenuation of radiation (i.e., with no mechanism for photobleaching or chemical amplification) can be limited by a maximum allowable contrast, sidewall angle, and ultimate resolution. This is because of the inherent absorption trade-off required when imaging into a resist film. Both maximum transmission (to reach to the bottom of the resist) and maximum absorption (to achieve the highest sensitivity) are desired. There is therefore an optimum resist absorbance value for any resist thickness.

It a resist film has a thickness t and dt is the thickness of the bottommost portion of the resist, the intensity transmitted through the film thickness to dt can be determined from Beer's law:

$$I = I_0 e^{-\varepsilon m t}, \tag{11.4}$$

where ε is the molar extinction coefficient of the sensitizer, and m is the molar concentration. The energy density absorbed at the bottom of the resist is

$$E = I_0 e^{-\varepsilon m t} \frac{(1 - e^{-\varepsilon m\, dt})}{dt}. \tag{11.5}$$

Because dt is small, $e^{-\varepsilon m\, dt}$ can be approximated as $I - \varepsilon m\, dt$ and

$$E = I_0 \varepsilon m e^{-\varepsilon m t}, \tag{11.6}$$

which is maximized when $\varepsilon m t = 1$. Converting to absorbance:

$$\text{Absorbance} = \log_{10} e \varepsilon m t = 0.434. \tag{11.7}$$

This is the optimum absorbance for a resist film regardless of thickness. In other words, higher absorption is desired for thinner resists and lower absorption is desired for thicker films. Resists for which chemical amplification or photobleaching is used introduce mechanisms that allow deviation from these constraints. The absorbance of a PAG for chemically amplified resist can be quite low because of the high quantum

yield resulting from acatalytic reactions. Photobleaching resists (such as DNQ/novolac) exhibit dynamic absorption properties, which can allow increased transmission toward the base of a resist film. For these resists, other absorption considerations are required.

The dynamic absorption that exists for DNQ occurs as exposure leads to a more transparent ICA photoproduct. This bleaching phenomenon can be described in terms of Dill absorption parameters *A*, *B*, and *C* [36]. The *A* parameter describes the exposure-dependent absorption of the resist, the *B* parameter describes the exposure-independent absorption, and *C* describes the rate of absorption change or bleaching rate. For a DNQ/novolac resist, the *C* parameter is conveniently related directly to resist sensitivity because photobleaching corresponds to the conversion of the photoactive compound (PAC) to the photoproduct (see Chapter 2 for a more detailed discussion of parameter characterization and modeling). The choice of a specific DNQ compound for mid-UV lithography needs to include evaluation of the unique *A*, *B*, and *C* parameters at the wavelength of exposure. It is generally desirable to have low exposure-independent absorption (*B* parameter) to achieve maximum exposure efficiency to the bottom of a resist layer. Several approaches exist to minimize residual *B* parameter absorption of DNQ/novolac resists [37]. These have included the use of highly transparent backbones for multifunctional PACs and binding of the sensitizer to the novolac polymer. A larger *C* parameter is also desirable for maximum sensitivity. Figure 11.7 shows absorbance spectra for two DNQ/novolac resists. Based only on the evaluation of the absorption properties of these two resists, it can be expected that the resist with smaller *B* parameter and

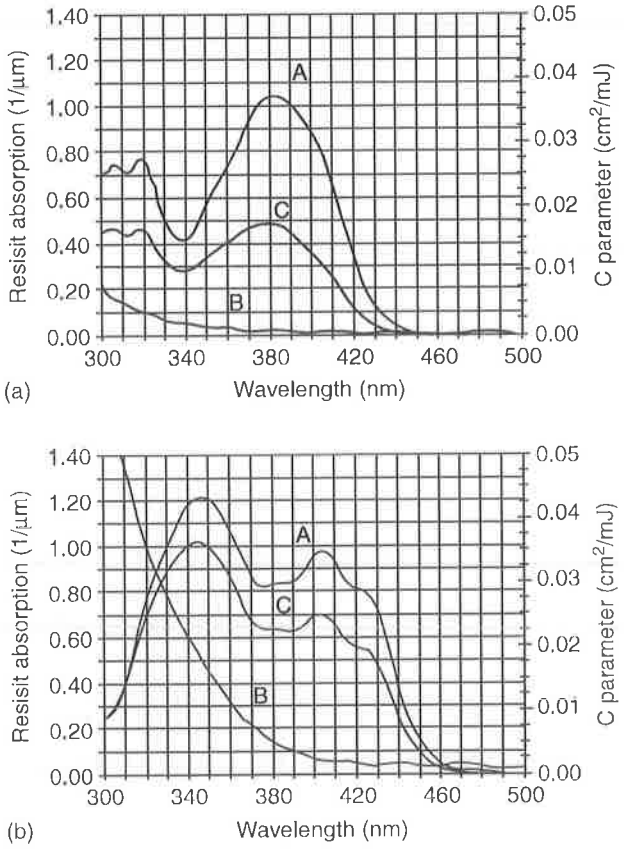

FIGURE 11.7
Absorbance curves for two DNQ/novolac resists showing Dill *A*, *B*, and *C* parameters. Resist (a) exhibits lower residual absorption (*B* parameter) at 365 nm whereas resist (b) has higher bleachable absorbance and speed (*A* and *C* parameters) at 436 nm. (From Prolith/2 V.5.0, 1997.)

larger A and C parameters may perform better (at a specific exposure wavelength) in terms of sensitivity, sidewall angle, and contrast.

Chemical amplification is another avenue that exists to improve the absorption characteristics of a resist. With quantum efficiencies several orders of magnitude higher than what can be achieved for direct photomodified resists, only a small amount of photon absorption is needed. This can be quantified in terms of A and B parameters, which may be on the order of 0.30 μm^{-1} compared with the 0.90 μm^{-1} levels encountered with i-line materials. The downside of such high transparency for resist materials is the increased opportunity for substrate reflection to degrade performance. The effects can be manifested as a linewidth variation over reflective steps (nothing) and a sidewall standing wave. Figure 11.8 shows standing waves resulting from the coherent interference of incident and reflected radiation within a resist layer. Reduction of these standing waves is crucial to retain critical dimension (CD) control. This can be dealt with in either resist exposure or process stages and is ordinarily addressed in both. To reduce standing wave effects during exposure, the reflected contribution to exposure must be controlled. This can be accomplished by incorporating a dye in the resist formulation. Dyes such as coumarin or curcumin compounds have been used as additives to DNQ/novolac resists and are very effective at reducing the reflected exposure contribution in a resist layer at g-line and i-line wavelengths. By adding a dye, the exposure-independent absorption (B parameter) increases. The result will be a decrease in reflection effects and standing waves and also a decrease in the amount of energy transferred toward the bottom of the resist. This will result in a decrease in sidewall angle, resist contrast, and sensitivity. Dyed resist for i-line use is therefore usually limited to highly reflective, noncritical layers.

Dyes that play a role in the chemistry of a resist system have also been introduced. By transferring the energy absorbed by a dye to the photosensitive component of a resist (for instance, through energy transfer or photoinduced electron-transfer mechanisms), an active dye can allow reduction of reflection effects while maintaining sensitivity and resolution. This has been accomplished in chemically amplified PHOST resists [38]. The resultant increase in the resist B parameters in this case leads to an increase in photoinduced chemical activity, yielding minimal loss in resist performance. Loading of such photoactive dyes can be determined from the preceding analysis for static absorption resists. Resist absorbance on the order of 0.434 could be expected to be best suited for optimal throughput. An alternative to

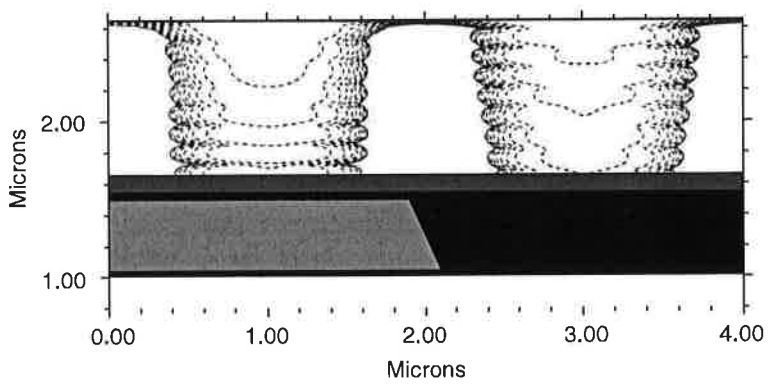

FIGURE 11.8
Resist standing waves resulting from coherent inference of incident and reflected radiation within a resist layer. Standing wave phase and amplitude is dependant on the underlying substrate.

dye incorporation is the use of an antireflective layer on the resist. The requirements of current IC processes will soon demand that substrate reflectivity be reduced to levels below 15 for critical layers. The use of such antireflective coatings (ARCs) has become a popular practice for *i*-line and DUV lithography and is discussed in more detail in Chapter 12.

11.6.2 Resists Exposure and Process Performance

The sensitivity (E_0) described earlier is a bulk resist characteristic that is useful for resist process comparisons or non-feature-specific process optimization. Resist E_0 swing curves allow, for instance, the determination of optimum coating thickness values. Monitoring of clearing dose requirements is also useful for characterization of exposure or development uniformity. Through the use of an exposure response curve, as shown in Figure 11.9, two additional bulk resist parameters can be obtained that allow further process characterization. Normalized thickness (normalized to initial predevelopment thickness) is plotted as a function of $\log_e$ exposure for a positive resist of a given thickness, exposed and developed under process conditions. An area of linearity exists in the logarithmic relationship, which can be characterized using a single contrast term:

$$\gamma = \frac{\Delta t/t_0}{\Delta \ln(\text{dose})}, \tag{11.8}$$

where t is thickness and t_0 is the initial coating thickness. Resist sensitivity or clearing dose (E_0) is the point on the exposure dose axis at which the normalized thickness become zero. A third parameter that is useful for describing resist capability is a normalized thickness loss parameter (t_ℓ), which is an indication of the amount of resist erosion that occurs in unexposed regions (also called *dark erosion*). An exposure response curve can be generated uniquely for any resist/development process, can be obtained from a more general development process, or can be obtained from a more general development rate curve, described in greater detail in Section 11.8. Figure 11.10 shows a development rate curve, where resist dissolution rate is plotted as a function of $\log_e$ exposure dose for a positive resist. As exposure is increased, the dissolution rate increases. The linearity of this relationship can be realized on a log–log plot, but a lognormal plot is used here to demonstrate the relationship between a development rate and exposure response curve.

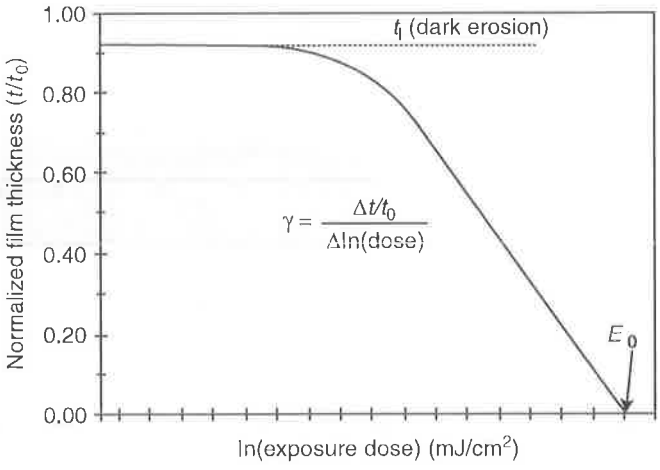

FIGURE 11.9
Normalized thickness as a function of $\log_e$ (exposure) for a positive resist of a given thickness, exposed and developed under specific process conditions. An area of linearity exists in the logarithmic relationship that can be characterized using a single contrast term (γ). Resist clearing dose (E_0) is the point on the exposure dose axis where normalized thickness becomes zero and the normalized thickness loss (t_ℓ) is an indication of the amount of resist erosion that occurs in unexposed regions.

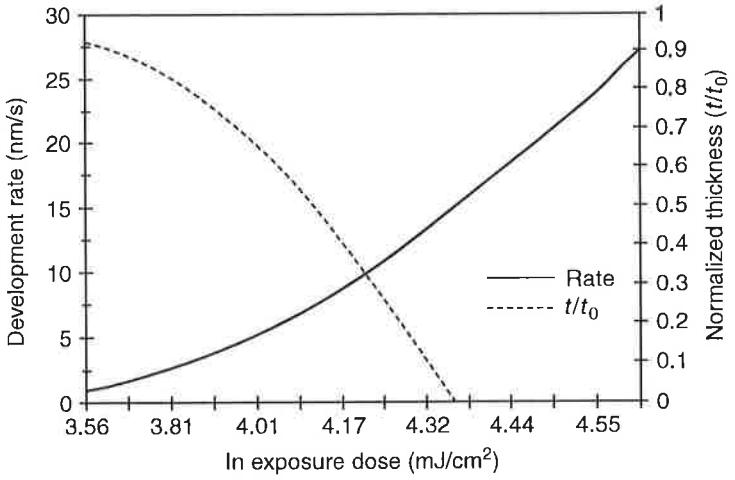

FIGURE 11.10
Resist dissolution rate (nm/s) plotted as a function of $\log_e$ (exposure dose) for a positive resist. Plotted also is an exposure response curve for this resist coated at 9000 Å and developed for 60 s.

Plotted along with dissolution rate in Figure 11.10 is an exposure response curve for this resist coated at 9000 Å and developed for 60 s.

11.6.3 Exposure and Process Optimization

To determine the optimum exposure dose (or range of doses) for a resist process, bulk resist characterization needs to be augmented with feature-specific characterization. To accomplish this, process specifications must be defined uniquely for each feature type and size, mask level, substrate, resist, and process. This is often a difficult task because definition on an optimum process requires operation at a near-optimum level. The task is therefore an iterative one that can often be made easier through the use of lithographic simulation tools.

Consider the focus-exposure matrix in Figure 11.11. Here, 0.5-μm dense lines are imaged into an *i*-line resist with a projection system at a partial coherence of 0.5. Resist CD is plotted against focal position for a series of exposure dose values. The nominal focus setting is labeled 0.0 and is typically at a point near 30% from the top surface, depending upon the resist refractive index and, to a lesser extent, upon NA and σ (for high NA values). At this position, t here is an optimum exposure dose for printing a biased mask CD to its targeted size (see Chapter 3 for a description of mask biasing). As focal position is changed, the feature no longer prints at the target value; it is either too small or too large. The adverse influence of overexposure is also increased. This can be understood by considering an aerial image as it is varied through focus, as shown in Figure 11.12. At best focus, a relatively large range of exposure variation can be tolerated. As defocus increases, a small amount of overexposure can result in a large amount of energy in shadow areas. Underexposure can result can result in insufficient energy in clear areas. An exposure must be chosen, therefore, to allow the greatest range of usable focus that results in a CD that remains within the specified target range. More appropriately, a specification is placed on the required exposure latitude to account for within-field-to-field nonuniformities. Together with tolerance limits on CD, a resulting usable depth of focus (UDOF) can be determined. For instance, for a $\pm 10\%$ exposure latitude requirement and a $\pm 10\%$ specification on CD, the optimum exposure from Figure 11.11 is

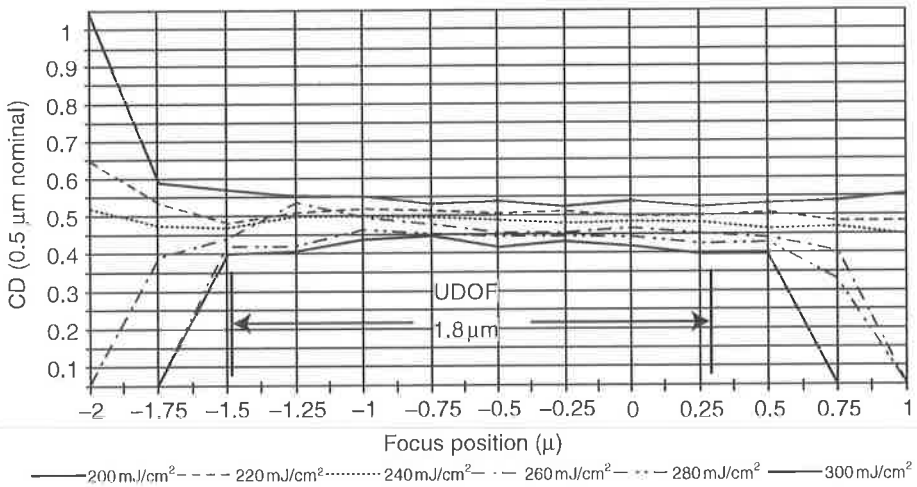

FIGURE 11.11
A focus-exposure matrix for 0.5-μm dense line features in a positive *i*-line resist over polysilicon using a numerical aperture of 0.45 and partial coherence of 0.60. Resulting usable depth of focus (UDOF) is 1.8 μm for a CD specification of ±1 and an exposure latitude requirement of 20%. The corresponding k_2 value for this single layer resist process is near 0.5.

240 mJ/cm^2 and the UDOF is near 1.8 μm. The resulting UDOF needs to be evaluated with respect to device topography. It should also be noted that any change in resist process will influence the focus. Any process enhancement methods, whether optical or chemical, have the potential to improve focal depth. These can include the use of reflection suppression (e.g., with an ARC), modified PEB, enhancements of contrast, and improvements in developer selectivity. For evaluation purposes, it is convenient to express a normalized UDOF through use of the Raleigh DOF k_2 factor:

$$k_2 = \frac{(\text{UDOF})(\text{NA}^2)}{2\lambda}. \tag{11.9}$$

The corresponding k_2 factor for the focus-exposure matrix of Figure 11.11 is near 0.5. Generally, single-layer resist processes can produce k_2 in the range of 0.4–0.6.

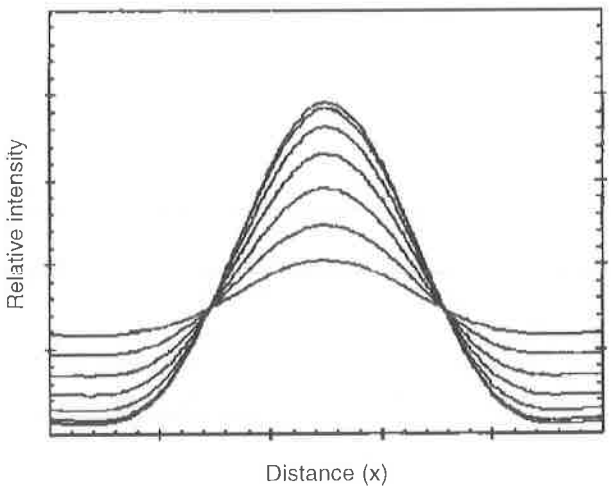

FIGURE 11.12
Through-focus aerial images for $\pm\lambda/\text{NA}^2$ of defocus. Images with no defocus can tolerate a large exposure variation. As defocus is increased, the choice of optimum exposure becomes more critical.

If a resulting k_2 does not correspond to UDOF values large enough for device topography, techniques of planarization may be required. Polymeric planarization is one alternative but is generally not considered robust enough to allow adequate process latitude for high-resolution IC applications. Chemical mechanical polishing (CMP) techniques, in which substrate surfaces are polished to reduce topography, are becoming commonplace in many IC process operations. From a lithographic standpoint, CMP can be considered as operation that allows improvements in focal depth, CD tolerance, and exposure dose control.

A focus-exposure matrix can also be generated for resist sidewall angle, although this is much more difficult task than for CD. Figure 11.13a shows a sidewall angle focus-exposure matrix and Figure 11.13b shows the corresponding array or resist feature profiles. At an optimum exposure dose value, the base CD of the features remains tightly controlled. At negative values or focus (corresponding to the bottom of the resist), there is a widening at the base of features. At positive focus values (toward the lens), feature thinning occurs. To evaluate the impact of these changes through focus and exposure, subsequent etch process selectivity and isotrophy need to be considered. If overexposure or underexposure is used to tune CD over topography (corresponding to a shift in focal position), it is

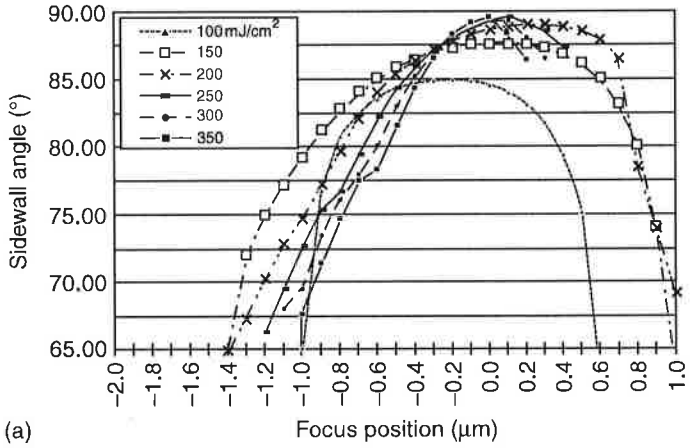

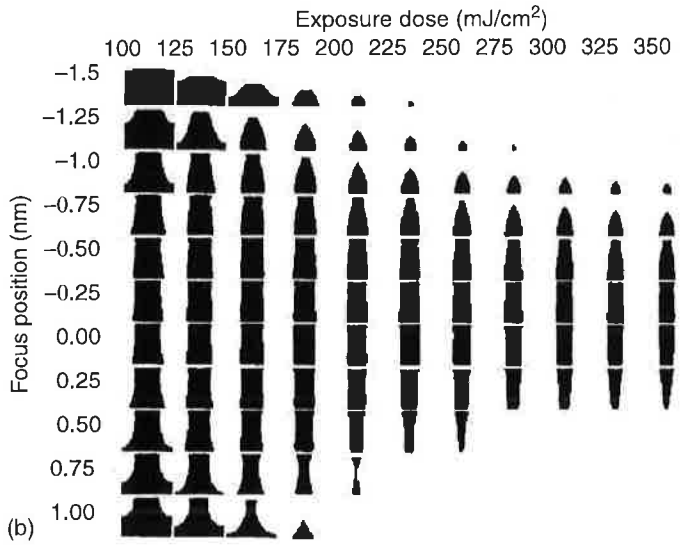

FIGURE 11.13
(a) A sidewall angle focus-exposure matrix. UDOF can be determined from a sidewall angle specification and exposure latitude requirements. (b) Corresponding array or resist feature profiles.

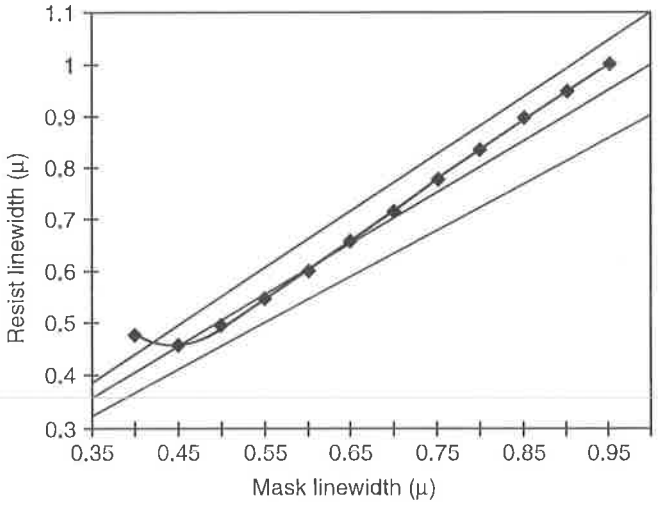

FIGURE 11.14
Plot of mask CD vs. resist CD for an *i*-line resist process. As features approach 0.45 μm, the linear relationship between mask and resist feature begins to break down. Features in this region require unique mask biasing to print to their targeted size.

likely that the resulting feature sidewall angle will not be adequate. A general requirement for sidewall angle specification are angles greater than 85°.

From these types of features-specific process evaluation techniques, it can be understood why it is difficult to increase exposure throughput for a resist without adversely affecting overall performance. For features large enough that aerial image modulation is high (i.e., there is little energy in shadow regions and sufficient energy in clear areas), there will exist a good deal of exposure latitude and UDOF so that some degree of exposure tuning is possible. As features approach $R=0.5\lambda/NA$ in size, the situation becomes challenging for conventional binary masking and single-layer resists.

Linewidth linearity has already been discussed as it applies to optical imaging systems. Photoresist materials also behave with a nonlinear response to exposure, which can be seen in the exposure response and development rate curves in Figure 11.9 and Figure 11.10. These nonlinearities can be used to take advantage of the lithographic process. Because the modulation need for small features is much lower than for large features, it would be expected that a resist that reacted linearly to exposure would do a poor job of faithfully reproducing mask features below $1\lambda/NA$ in size. By tailoring the exposure and dissolution response properties of a resist to operate in a specific desirable nonlinear fashion (nonlinearity itself does not imply added capability), the linearity of the entire lithographic process can be improved. Figure 11.14 shows a plot of resist CD vs. mask CD for an *i*-line resist process. Only as features approach 0.45 μm in size does the linear relationship between the mask and the resist feature begin to break down. Features in this region require unique mask biasing to print to their targeted size. The situation becomes more complex as various feature types are considered and resist linearity down to the minimum size of device geometry is desirable

11.7 Postexposure Bake

A postexposure bake (PEB) of a DNQ/novolac resist brings about chemical and physical actions similar to those for prebake. By subjecting resist films to a predevelopment bake

step at a temperature higher than used during prebake, some DNQ decomposition prior to exposure can be reduced. By baking exposed resists at temperatures on the order of 5°C–15°C higher than prebake temperatures, solvent content can be reduced from 4%–7% (prior to exposure) to 2%–5%. Whereas prebake is generally performed to bring the resist into region II in Figure 11.5, the elevated temperatures used for PEB places the resist toward region III. The most beneficial consequence of a PEB step is, however, not an extended action of earlier bake steps, but instead a significant impact on standing wave reduction via thermal flow [39]. During exposure over a reflective substrate, coherent interference produces a distribution of intensity within the resist film. The nodal spacing is a function of the resist refractive index (n_i) and wavelength:

$$\text{Distance between nodes} = \frac{\lambda}{2n_i}. \tag{11.10}$$

The amplitude of the resist standing wave will be affected by absorbance of the resist (α, which may be dynamic if resist bleaching occurs), resist thickness (t), and reflectance at the resist-air (R_1) and resist-substrate (R_2) interfaces [40] resulting in a wing effect where

$$\text{Standing wave "swing"} = 4\sqrt{R_1 R_2}\exp(-\alpha t). \tag{11.11}$$

Interface reflectance values (R_1 and R_2) are determined from the complex refractive index values of the media involved:

$$\text{Reflectance} = \left(\frac{n_a^* - n_b^*}{n_a^* + n_b^*}\right)^2. \tag{11.12}$$

In addition to resist and substrate contributions to interference effects, exposure source characteristics need to be considered. The coherence length (l_c) for a radiation source is determined on the basis of the source wavelength (λ) and bandwidth ($\Delta\lambda$) as

$$l_c = \frac{\lambda^2}{\Delta\lambda}. \tag{11.13}$$

As the resist thickness approaches the source coherent length, interference effects (standing waves) become negligible. A typical coherence length for *i*-line stepper tools may be on the order of 10 μm. For a 248-nm lamp-based step-and-scan system, I_c may be

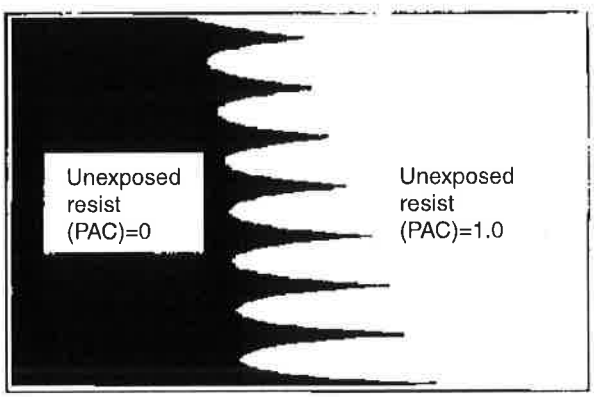

FIGURE 11.15
Distribution of photoactive compound (PAC) as a result of standing-wave resist exposure. Unexposed regions of the photoresist contain PAC, exposed regions contain photoproduct. Because the resist temperature is near or above its T_g, the PAC can effectively diffuse through the polymer matrix to reduce the effective standing wave in the developed resist sidewall.

on the same order, but as excimer laser lithography is pursued, a 10^3–10^4 factor increase occurs. Although it is not expected that a resist would be coated to thicknesses approaching 10 μm or more, the analysis offers insight into the increasingly critical concern with standing wave control. Considered together with the higher transparency (low α) of a chemically amplified resist, it becomes obvious that resist imaging over reflective substrates using an excimer laser source would be difficult without employing means of control or compensation.

To demonstrate the impact that a PEB step can have on resist standing waves, consider Figure 11.15. Unexposed regions of the photoresist contain a photoactive compound, exposed regions contain photoproduct, and the boundary between them is determined by the constructive and destructive interference nodes of the exposure standing wave. If the resist temperature is near or above its T_g, the PCA can effectively diffuse through the polymer matrix and produce an averaging effect across the exposed/unexposed boundary. This PAC diffusion is a function of the resist T_g, the PAC size and functionality, bake time and temperature, remaining solvent concentration, resist free volume, and (for DNQ/novolac, for instance) any binding between the resin. Figure 11.16 shows the resist standing wave pattern as a function of the PAC diffusion length.

For chemically amplified resists based on thermally induced acid reactions, PEB is used to accomplish critical chemical stage and must be considered nearly as critical as exposure in terms of control, uniformity, and latitude requirements. The concept of a bake "dose" control is a convenient comparative metric to exposure dose control for acid-catalyzed deprotection (positive resists) or cross-linking (negative resists). An Arrhenius relationship exists between PEB and exposure, such as that shown in Figure 11.17 [14]. Here, log (exposure dose) is plotted against 1/PEB, from which an effective E_a can be determined. Whereas exposure uniformity on the order of ~1% is a current requirement for resist

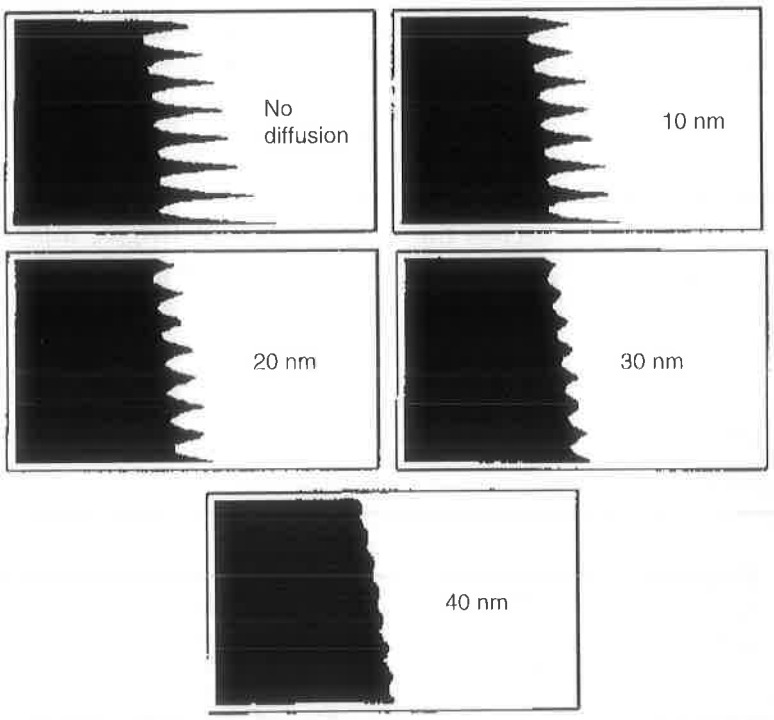

FIGURE 11.16
Simulated standing-wave pattern in developed resist as a function of increasing PAC diffusion length.

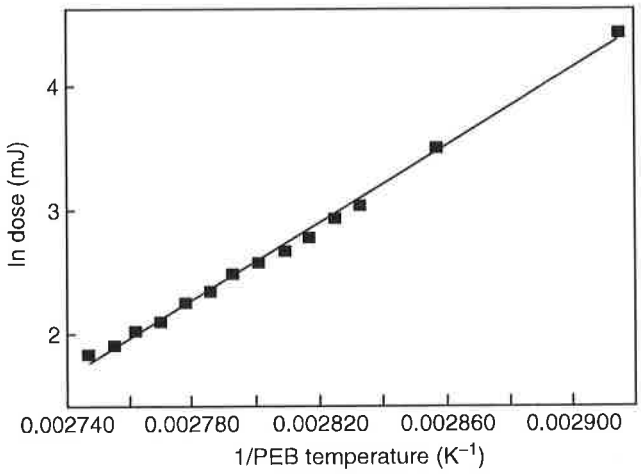

FIGURE 11.17
Arrhenius plot or resist sensitivity vs. PEB temperature for a DUV CAR resist. Dose required to print 0.5-μm lines with a 90-s bake is plotted against 1/PEB temperature. An effective activation energy can be calculated from such a plot (130 kJ/mol in this case). (From Sturdevant, J., Holmes, S., and Rabidoux, P., *Proc. SPIE*, 1672, 114, 1992.)

exposure tools, it can be expected that PEB control should be at least as critical. The rate of these reactions is a function of the acid concentration, the activation energy of the protected polymer, the diffusivity of the acid, and the PEB conditions.

Acid diffusion in PHS chemically amplified resists is generally on the order of 50 to a few hundred angstroms, limited by resolution requirements. If neutralization of acid occurs, the exposed resist dissolution rate decreases. If environmental contamination occurs after exposure and prior to PEB, a thin, less soluble inhibition layer forms on the top surface of the resist, which results in the formation of a characteristic T-top upon development, as shown in Figure 11.18. Any delay between exposure and PEB (known as postexposure delay, PED) allows this phenomenon to occur. Early material PED time requirements were on the order of a few minutes. Current generation resists allow delays up to several hours. It is important to realize, however, that acid neutralization can begin immediately upon exposure and performance must be evaluated for the specific resist process conditions and process tolerances. Low-E_a resists do not require elevated PEB temperatures for reaction, which can minimize the control requirements for this process step. These resists control tolerate high baking temperatures, which may introduce additional stability problems. Choice of the PAG is less critical, allowing choices with smaller cross-sections than those needed for high-activation-energy materials. Diffusion

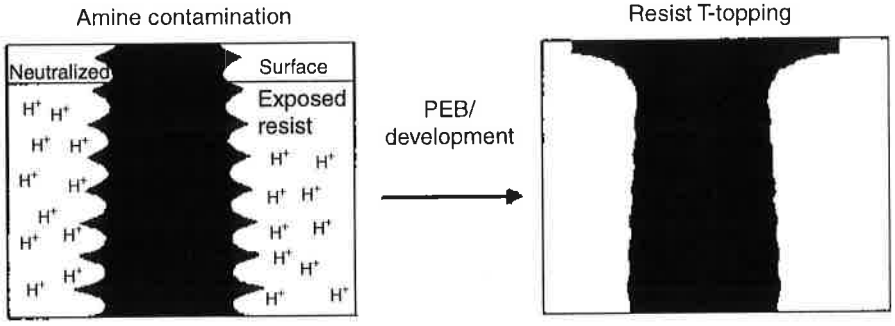

FIGURE 11.18
Environmental amine contamination of a chemically amplified (PHS) resist resulting in "T-top" formation after development.

properties are also based on size and should be evaluated uniquely for resists of either category.

When determining PEB requirements for deprotection, postexposure solvent content and polymer density also need to be taken into consideration. Temperature control on the order of 0.1°C may be required, with uniformity needs on the same order over wafer diameters approaching 300 mm. Material improvements may relax this requirements somewhat, but control to a few tenths of a degree can be expected as an upper limit.

An additional improvement brought about through the use of a PEB step is a potential increase in resist development rate properties, specifically the dissolution rate log slope (DLS) as discussed in the development section [42]. This occurs as a result of the decrease in resist dissolution rate especially at the resist surface, which is more pronounced in some resists than in other. By reducing the surface dissolution rate, unexposed film erosion can be reduced, resulting in an increase in sidewall slope and an improvement in process latitude. The surface modification is a result of solvent loss and a possible surface "skin" effect, enhanced by resist modification at elevated temperatures.

For optimal process performance, PEB processes for chemically amplified PHOST resists cannot be considered separately from soft bake steps. There are trade-offs between high and low levels of each. During soft bake of a chemically amplified PHOST-based resist, standing waves can be reduced through use of lower temperatures, which allow an increase in acid diffusion across the exposed/unexposed resist boundary. To reduce T-top formation, a high PEB is also desirable. Through use of high PEB temperatures, deprotection can occur even with some degree of reduced acid concentration at the resist top surface. This low soft bake, high PEB combination can result in additional undesirable phenomena. When the resist film is allowed to retain a relatively low T_g, pattern deformation can result from rapid PHOST deprotection and subsequent gas evolution at high PEB temperatures. A stepwise PEB has been suggested as a possible solution [43]. An initial low-temperature stage removes protective groups from the bulk of the resist with minimum deformation. A high-temperature stage follows to enhance top-surface deprotection and reduce T-top formation.

As discussed earlier, intrinsic or added free volume will affect the glass transition and dissolution properties and deprotection mechanisms of phenolic-based photoresists. The CAR deprotection reaction itself has also been shown to contribute additional free volume [44]. Exposure of PEB-induced variation in resist density can affect dissolution uniformity and CD control. This added influence of exposure and PEB can lead to complex relationships and increased control requirements. The deprotection and densification mechanism can best be separated in resist systems with low activation energies.

11.8 Resist Development

Resist systems based on solvent development, such as cross-linking bis(arylazide)-*cis*-polyisoprene negative resists, require some degree of swelling to allow removal of soluble polymer chains or fragments [46]. To keep resist pattern deformation to a minimum, a series of solvents is generally needed for development, with careful consideration of kinetic and thermodynamic properties [46]. The development of resists based on novolac, PHOST, or other acrylic resins involves similar dissolution stages but does not require such adverse swelling for dissolution [47–49].

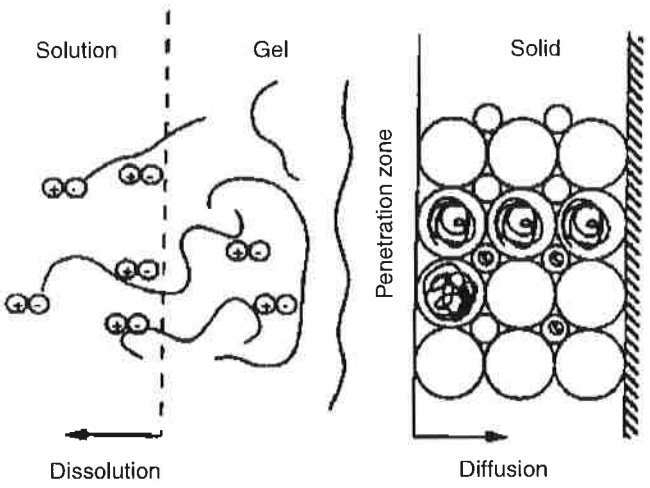

FIGURE 11.19
Diagram of a three-zone novolac dissolution model with a gel layer containing water, base, and hydrated, partially ionized novolac chains; a penetration zone.

11.8.1 Dissolution Kinetics of Phenolic Resin Resists

In novolac resins, a narrow penetration zone is formed as water and hydroxyl groups are incorporated in the novolac matrix. This zone is rate limited and does not encompass the entire resist layer, allowing dissolution of resist with minimal swelling. Following the formation of this intermediate layer, phenol is deprotonated and the resulting phenolic ion reacts with water. The negative charge of the phenolate ion is balanced by the developer cations. Upon sufficient conversion of phenol groups, the polymer is soluble in aqueous alkaline developer. A three-zone model has also been suggested, as shown in Figure 11.19 [50]. These zones exist during novolac development:

1. A gel layer containing water, TMAH (base), and partially ionized novolac. The thickness of this layer depends on depends on agitation, novolac microstructure, and the developer cation.
2. A penetration zone with a low degree of ionization. The thickness of this zone also depends on the novolac structure as wall as the developer cation size and hydrophobicity.
3. Unreacted bulk novolac resist.

The resulting dissolution rate of a resist material is determined by the formation of the gel and penetration layers and the subsequent dissolution of the gel layer into the developer.

In DNQ/novolac resists, exposure of the PAC leads to photoproduction of ICA, which acts as a dissolution accelerator. First-order kinetic models for development are based on this mechanism (see, for instance, Chapter 2). DNQ in sufficiently high concentrations (5–25 wt%) also acts as a dissolution inhibitor or the phenolic novolac resin, decreasing its hydrophilic nature (enhanced development models described in Chapter 2 also account for this phenomenon). This inhibition effect can also be accomplished with other compatible compounds and it not limited to DNQ. It might be reasoned that a similar mechanism would exist for PHOST resins, but this is not the case. Although the dissolution of novolac can be decreased when combined with DNQ by as much as two orders of magnitude, the high dissolution rate of PHOST is not significantly reduced. This can explained by considering the hydrophilic nature of both materials. Novolac is, for the most part, a hydrophobic resin with hydrophilic sites created when developer reacts with hydroxyl

groups. These phenolate ion positions allow a diffusion path for development. The sites of hydroxyl groups are only potential hydrophilic sites that can be tied up or isolated by the polymer's large aromatic rings. PHOST is a vinyl polymer with no aromatic rings in the backbone. Hydroxyl groups exist in a "corkscrew" configuration along the polymer chain, allowing very effective diffusion paths and extremely high dissolution rates.

The dissolution kinetics of chemically amplified resists based on PHOST are also quite different from those for DNQ/novolac. Whereas the dissolution of novolac resins is determined by two competitive reactions (inhibition by the DNQ and acceleration resulting from the developer-induced deprotonation of the novolac), there is one primary rate-determining stage for two-component PHOST chemically amplified resists. A similar developer-induced deprotonation of phenolic hydroxyl groups has been shown to dominate for negative resists, whereas developer penetration into hydrophobic *t*-BOC-protected PHS is rate determining for positive resists [51].

11.8.2 Development and Dissolution Rate Characterization

Development of conventional resist materials is based on imagewise discrimination. To understand and optimize photoresist development, it is necessary to characterize exposure-dependent dissolution properties. As discussed earlier, the extraction of development rate and exposure relationships allows tremendous insight into the imaging capabilities of a resist process. Shown in Figure 11.20 is a family of normalized thickness versus development time curves for a resist material exposed at various dose levels. Such curves can be obtained using laser interferometry techniques and separate substrate exposure [52,53] or a single substance and multiple exposures [54]. A development rate vs. exposure curve such as that in Figure 11.21 can be produced from a family of these dissolution curves. To characterize fully the dissolution properties of a resist throughout its entire thickness, a rate curve may not suffice, because development rate is a function of resist thickness. Surface inhibition reduces the development rate significantly at the top surface of the resist. Figure 11.22 shows a development rate vs. resist thickness curve demonstrating that development rate increases from the top surface of the resist toward the bottom.

When development rate and exposure are plotted in a log–log fashion, as shown Figure 11.23, a linear region exists that can be descried in terms of a development rate log slope (DLS):

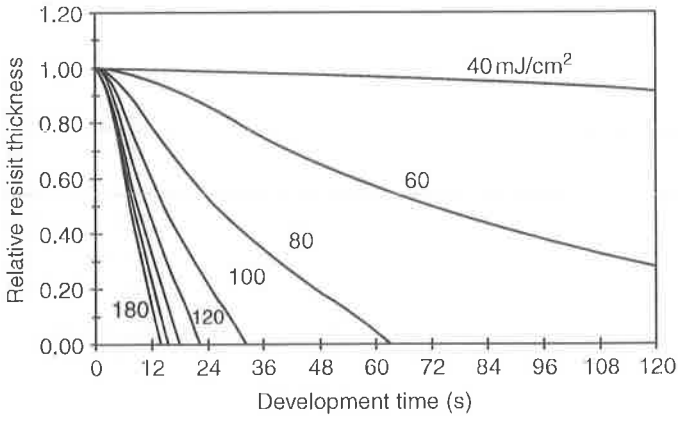

FIGURE 11.20
Normalized film thickness vs. development time curves for resist exposed at 40 to 180 mJ/cm^2. Selection of single development time values can lead to development rate vs. relative exposure curves.

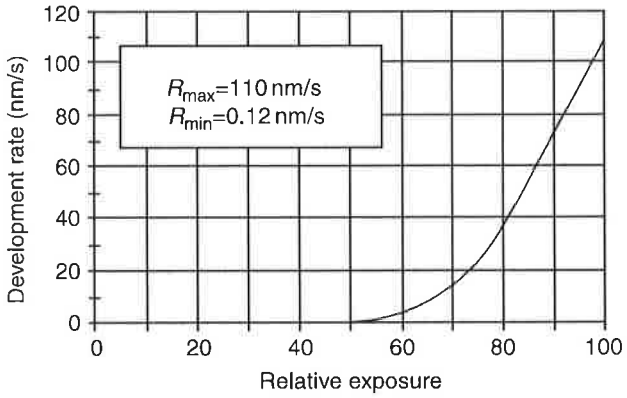

FIGURE 11.21
A development rate vs. relative exposure curve from Figure 11.20.

$$\text{DLS} = \frac{\partial \ln(\text{dev. rate})}{\partial \ln(\text{dose})}. \tag{11.14}$$

Dissolution rate contrast can be expressed as

$$\text{Contrast} = \frac{R_{max}}{R_{min}}, \tag{11.15}$$

where R_{max} and R_{min} are the maximum and the minimum development rates, respectively. Together, DLS and dissolution rate contrast are effective measures of the dissolution properties of a resist material. High levels of both metrics are desirable. Control of the resist and development properties can be used to some extent to influence performance. A moderate contrast value near 10,000 is generally sufficient. As development normality is changed, R_{max} and R_{min} are both affected (as long as base concentration does not fall below a critical level, pH ~12.5), but their ratio and the shape of the curve remain fairly constant [55]. The R_{max} is primarily a function of the polymer itself [55]. Major resist, sensitizer, and solvent factors that influence development rate include:

- Polymeric structure
- PAC/PAG/inhibitor structure
- PAC/PAG/inhibitor concentrations (DNQ/loading >20%)
- Protection ration (PHS protection ration >25%)

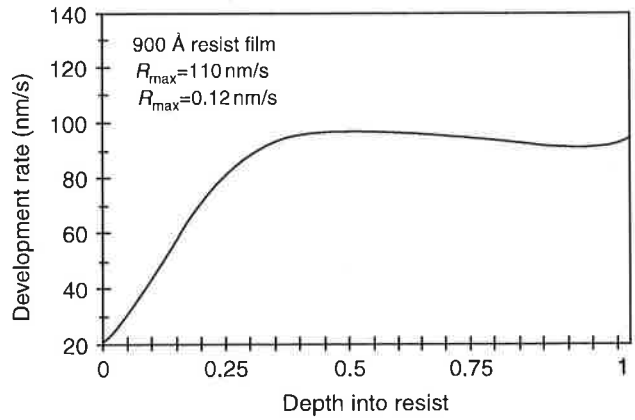

FIGURE 11.22
A development rate vs. resist thickness curves, showing distribution of dissolution properties through a resist film.

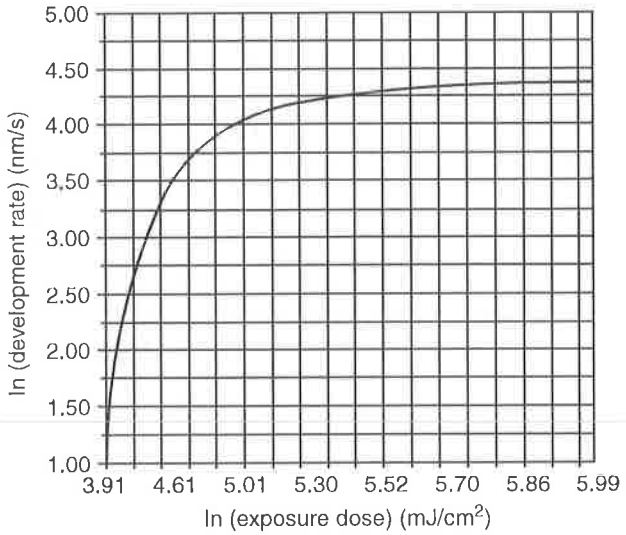

FIGURE 11.23
Log development rate vs. log exposure dose. Dissolution rate performance can be evaluated in terms of the slope of the linear region of the curve and the R_{max}/R_{min} ratio.

- Solvent concentration
- Polymeric molecular weight (greater than 1.3×10^4 g/mol)
- Polydispersity (less than 3)
- Developer composition (metal ion vs. TMAH)
- Developer cation size and concentration
- Resist surfactant
- Resist dissolution inhibition/acceleration state
- Developer surfactant

Hydroxyl group positions on PHOST polymer also affect the dissolution rate, a function of hydrogen bonding and steric hindrance with the polymer backbone [56]. Copolymers of 2-and 4-hydroxystyrene have been shown to allow control of PHOST dissolution properties.

11.8.3 Developer Composition

Phenolic strain-based resists can be developed using buffered alkaline solutions such as sodium metal silicates. These metal silicate developers yield a maximum development rate and low dark erosion, compared with most other developer choices. Possible metal ion contamination of devices has nearly eliminated the use of this class developer, however, in favor of metal-ion-free tetramethylammonium hydroxide (TMAH). Furthermore, standardization of TMAH developer formulations is becoming widespread because having no requirements for coexistence of several developer types is more economical and allows better quality control. The larger cross-section of TMH compared with NaOH leads to lower development rates, which may result in lower working sensitivities. TMAH developer concentrations in the range of 0.2–0.3 N allow sufficient sensitivity with high contrast and minimum erosion. A 0.26 N solution has become a standard for most overseas resist processing.

In addition to TMAH, surfactants are added to a developer to reduce development time and scumming. Surfactants are used as additives to photoresists, chemical etchants, and developers to improve surface activity or wetting. TMAH developers often employ

surfactants at the ppm level to reduce surface tension. Surfactants are especially useful for improving the dissolution of small-surface-area features such as contacts or small space features. By increasing the effective wetting of the developer, scumming problems can be minimized and overexposure- or overdevelopment-induced process biases can be reduced. Also, through the use of developer surfactants, initial development inhibition at the resist surface can be reduced. Additives used for resist developers are mainly of the nonionic variety with hydrophilic and hydrophobic structural characteristics, such as ethylene oxide/propylene oxide block polymer segments with molecular weights near 1000. Concentrations may be up to 800 ppm or 0.05 wt.%. Surface tension decreases as the concentration of surfactants increases until a critical micelle concentration (CMC) is reached. This CMC level represents an equilibrium state at which aggregation begins. Very small changes in the structure of surfactant molecules have been shown to result in large change in resist development performance. The number and location of hydroxyl groups in the molecular structure of surfactant determine the activity of surface dissolution during development [57]. The behavior of developer surfactants also depends on resist material properties. Resists that have a larger degree of surface hydrophobicity benefit most from surfactant additives and have been shown to be less dependent on surfactant type. The benefits gained for a particular resist therefore depend on unique resist and surfactant properties and interactions. Figure 11.24 shows how surface agents acting at a resist/developer interface enhance the surface activity by decreasing surface free energy [58].

In addition to the chemical composition of the developer, the concentrations of hydroxyl ions, developer cations, and anions have been shown to strongly influence the dissolution rate of pure novolac films [59]. As the cation concentration is increased, a linear increase in dissolution rate occurs at a constant pH, apparently independent of anion concentration [60]. The structure of the developer cation and anion will determine the maximum allowable concentration before a decrease in dissolution rate begins. Along with the dissolution dependence on the size of the developer cation, its hydrophilicity and T_g of the partially ionized novolac also influence the development rate [61].

Development temperature is important and requires tight control. This is true not only for the bulk development reservoir and plumbing but also for the development bowl and development atmosphere. The rate of dissolution for TMAH developers follows an

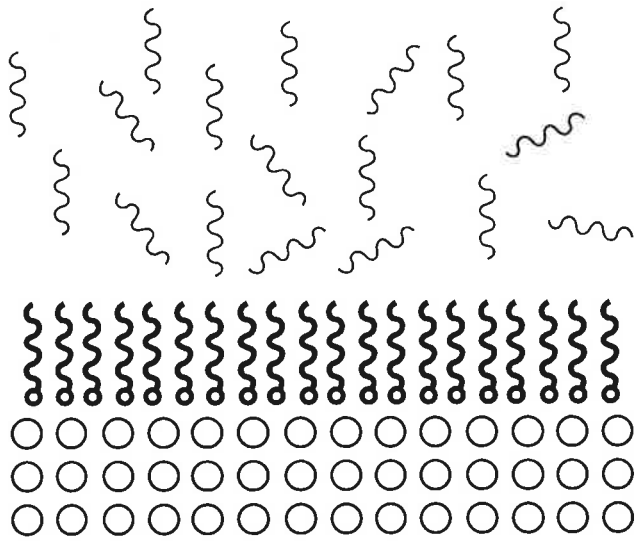

FIGURE 11.24
Orientation of surface molecules (center) at a hydrophobic (top)/hydrophilic (bottom) interface. The surfactant molecules are oriented so as to lower the interfacial free energy. (From Florus, G., and Loftus, J., *Proc. SPIE*, 1672, 328, 1992.)

Arrhenius relationship:

$$k = A_0 e^{-E_a/RT}, \tag{11.16}$$

with an apparent negative activation energy (E_a) [62]. The reason for this is a highly exothermic sequence of deprotonation steps. A decrease in development temperature results in increased activity, which may seem counterintuitive. This is not the case for development with NaOH or developers with similar chemistry because no exothermic reactions exist.

11.8.4 Development Methods

Resist dissolution properties are highly dependent on the development method employed. Development methods commonly used for conventionally coated wafer substrates include static immersion, continuous spray with slow rotation (~500 rpm), and stationary or slow rotation puddle development.

Spray development involves one or more spray nozzles to dispense developer toward the wafer substrate. Processes using ultrasonic atomization of developer allow relatively low velocity dispersion and minimal adiabatic cooling effects during the dispensing. For conventional spray development, the resist dissolution rate has been shown to be relatively insensitive to spray nozzle pressure but linearly dependent on spin speed [63]. With ultrasonic spray development, dissolution variation and resist erosion can result from poor control of the nozzle spray pattern. Dissolution rate and uniformity are also dependent on the uniformity of the spray pattern directed toward the wafer. To minimize nonuniformities, wafer chuck rotation must be carefully controlled at fairly low speeds (100–500 rpm) to ensure adequate developer replenishment. For these reasons, along with the excessive developer volume dispensed during processing, puddle processes are now most common for high-volume production.

Puddle development techniques can improve the tool-to-tool matching of development processes. In addition, the control of puddle development processes over time is significantly better. For optimal performance, flow is kept low to reduce variations in development rate at the edge of the wafer. The dispensed volume or developer should also be kept low to minimize chemical costs and back side wetting but not so low as to cause localized nonuniformities or scumming. The dispensed volume should be carefully controlled to ensure full and uniform coverage of the entire resist surface. During a puddle development process, slow rotation or single rotation may be used to disperse trapped air and provide agitation. If a surfactant-free developer is used, an increase in dispensing pressure may be required to enhance resist wetting.

There are several trade-offs to consider when making a choice between spray, puddle, and immersion methods. Although immersion development can lead to minimum erosion by physical removal of a resist, it is not well suited to the in-line processing that now dominates in production. During puddle development, chemical activity decreases with time as the small developer volume becomes exhausted, a situation that is not encountered during immersion processing. There is a more subtle difference between these two techniques as the depletion of developer additives is considered. At ppm levels, surfactants can be exhausted during static immersion development, significantly changing the chemical nature of the developer with time. Because puddle development introduces fresh chemistry for every wafer, consistent wafer-to-wafer development can be ensured. A multiple-puddle method of development [64] is now commonplace in wafer processing and usually involves tow development

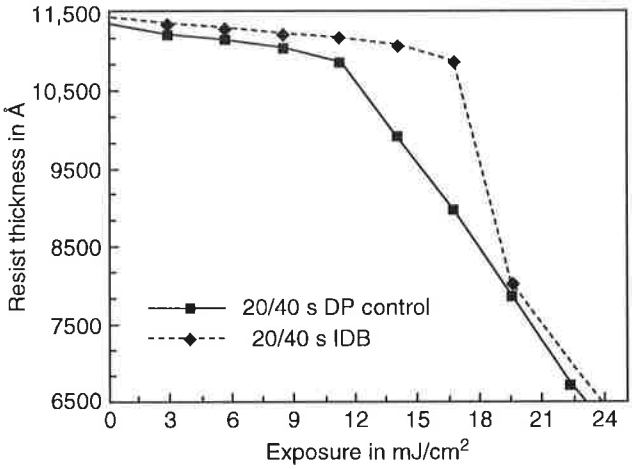

FIGURE 11.25
Resist film thickness vs. exposure dose for interrupted double-puddle (DP) development and for 50°C warm-water intermediate development bake (IDB) showing improvement in resist contrast with IDB. (From Damarakone, N., Jaenen, P., Van den Hove, L., and Hurditch, R., *J. Proc. SPIE*, 1262, 219, 1990.)

stages. The process consists of dispensing developer onto a wafer and allowing it to remain for a short time (10–20 s). It is then spun off and a second puddle is formed and allowed to complete the process (20–30 s). Although such multiple-puddle processes serve to replenish developer to the resist, the effect that makes this technique most attractive is an inhibition that occurs between development cycles. The dissolution of unexposed or partially exposed resist will be preferentially slowed at the location of the resist front after the end of the first development step. This phenomenon can be enhanced if rinse and spin-dry steps are added between development cycles [65]. The inhibition may be a result of base-induced oxidation or azo coupling of the novolac. It has also been suggested that a surface modification occurs with interrupted development and an increase in surface energy can enhance resist dissolution discrimination [66]. Multiple-development-step processing has been also reported and variations on these techniques are now widespread [67]. Intermediate development baking processes have also been investigated [68]. Figure 11.25 shows resist film thickness plotted as a function of exposure dose for double-puddle and warm-air intermediate development baking processes. Resist contrast is effectively increased with the use of the warm-air bake.

It is important to rinse remaining chemicals from the wafer surface after development because inadequate removal can result in high defect levels. Both a top-side rinse and a back-side rinse are needed to remove developer and contaminants that could be transferred to subsequent process steps.

11.8.5 Development Rate Comparison of *i*-Line and DUV Resists

Although similarities exist between the dissolution properties of DNQ/novolac and PHOST-based chemically amplified resists, comparison of these materials demonstrates salient differences in their performance and capabilities. Development rate curves are the tool best suited for this type of comparison. Shown in Figure 11.26 are development rate curves for an *i*-line DNQ/novolac resist, a negative DUV chemically amplified resist, and a positive DUV chemically amplified resist [69]. The negative DUV resist is a three-component acid-hardening resist based on a phenolic resin (PHOST), a melamine cross-linker, and a photoacid generator [70]. The positive DUV resist is a *t*-BOC-protected PHOST and a photoacid generator [71]. The rate curve for the *i*-line resist (Figure 11.26a) shows

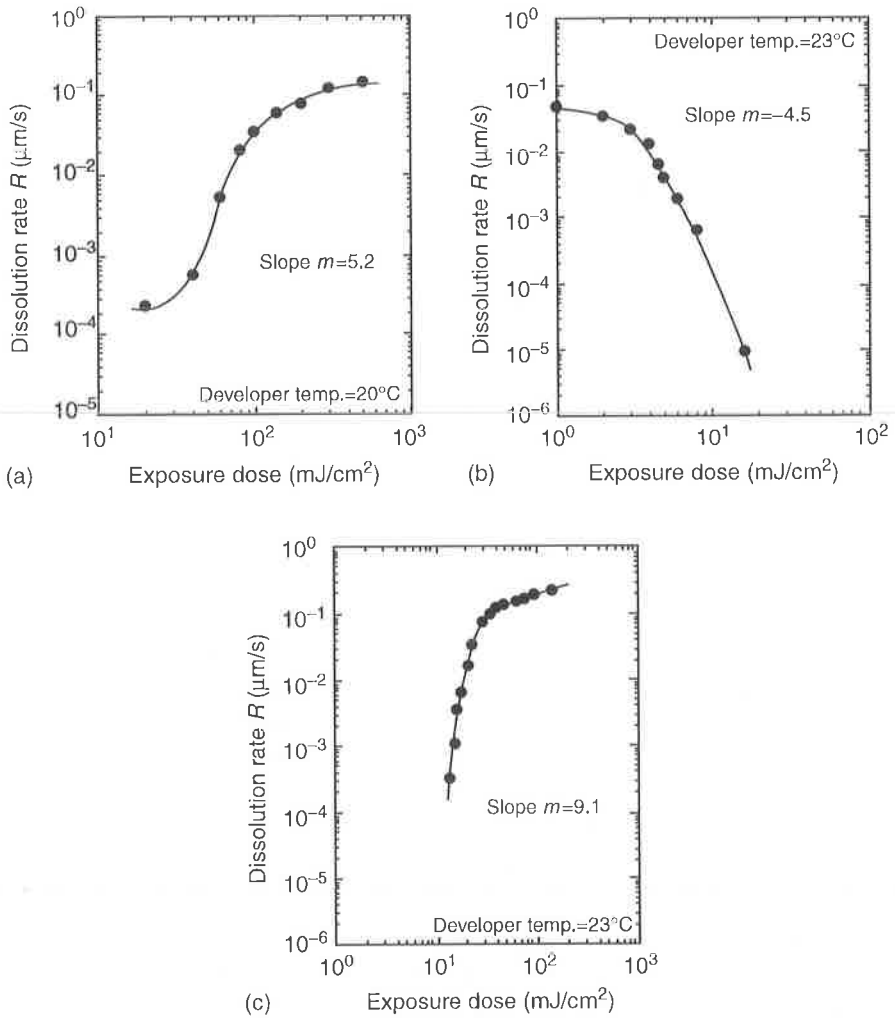

FIGURE 11.26
Log development rate curves for (a) an *i*-line DNQ/novolac resist; (b) a negative DUV chemically amplified resist; and (c) a positive DUV chemically amplified resist. Slope is the development rate log slope (DSL). (From Itani, T., Itoh, K., and Kasama, K., *Proc. SPIE*, 1925, 388, 1993.)

a nonlinear dissolution rate that can be divided into three regions. The ability of this resist to achieve high contrast (γ) is evident from the steep development rate log slope (DLS). A large development rate contrast (R_{max}/R_{min}) also exists, leading to high sensitivity and low erosion properties. Figure 11.27a shows an Arrhenius plot for this resist, where distinct regions also exist: (I) a high dose, low-temperature region where E_a is small and positive, (II) an intermediate region where E_a is negative and decreasing, and (III) a low-dose, high-temperature region where E_a is positive and comparatively large. These results can be compared with the development rate curves for the negative DUV resist (Figure 11.26b and Figure 11.27b). In this case, a moderately high DLS exists, and when compared with the *i*-line resist, it would be expected to coincide with worse lithographic performance. The Arrhenius plot shows a constant E_a and suggests that only one reaction mechanism governs development rate. Figure 11.26c and Figure 11.27c show plots for the positive DUV resist. The DLS value is much greater than that for either the *i*-line or the negative resist. The Arrhenius plot also suggests a single dissolution mechanism, but a saturation of E_a appears to exist at higher doses. At these high doses, deprotonation of

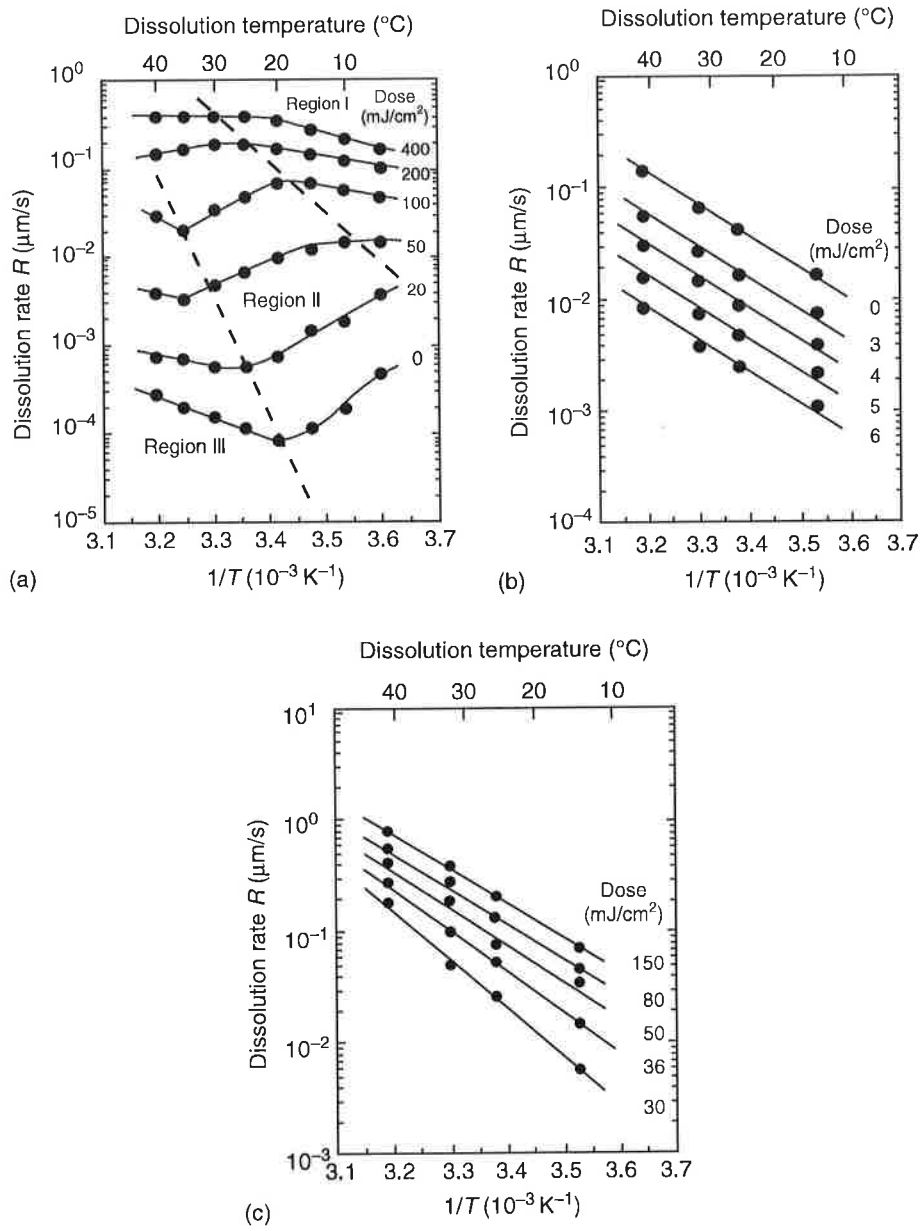

FIGURE 11.27
Arrhenius plots for the three resists in Figure 11.26: (a) an Arrhenius plot for the *i*-line resist where three distinct regions exist; (I) a high dose/low temperature region where E_a is small and positive, (II) an intermediate region where E_a is negative and decreasing. and (III) a low dose/high temperature region where E_a is positive and comparatively large; (b) a constant E_a for the negative CAR suggests that only one reaction mechanism governs development rate; and (c) suggests also a single dissolution mechanism for the positive CAR but a saturation of E_a appears to exist at higher doses where nation of hydroxyl groups at the PHOST becomes rate determining, similar to the mechanism for the negative resist. (From Itani, T., Itoh, K., and Kasama, K., *Proc. SPIE*, 1925, 388, 1993.)

hydroxyl groups at the PHS becomes rate determining, as in the mechanism for the negative resist. Figure 11.28 shows the proposed dissolution model for the positive DUV chemically amplified resist. Figure 11.29a and b show development rate curves for a three-component positive DUV resist that includes an additional dissolution inhibitor and various *t*-BOS protection levels and molecular weights [72]. Shown in Figure 11.30 are

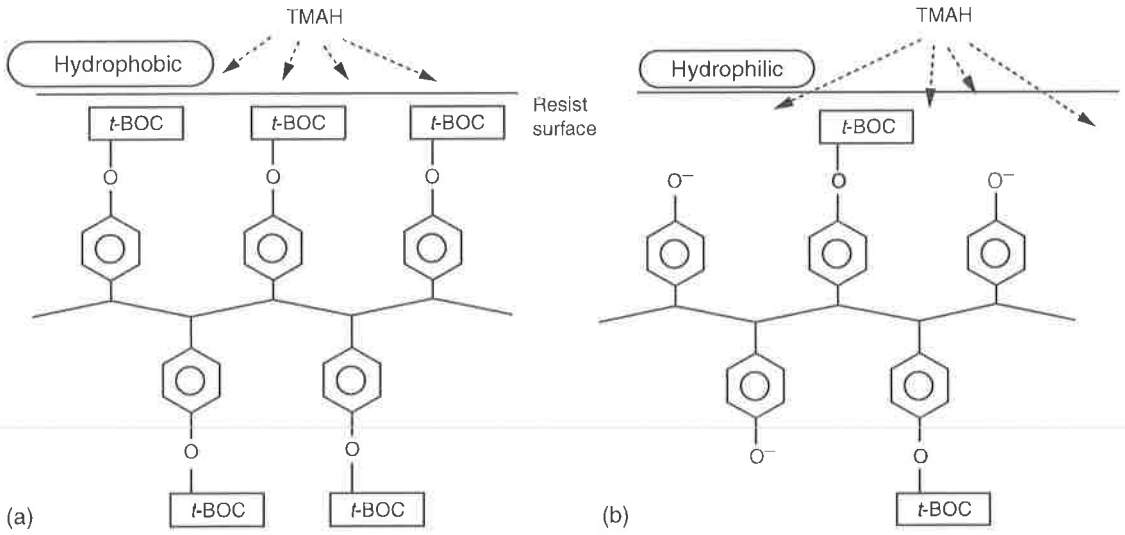

FIGURE 11.28
A proposed dissolution model for positive DUV chemically amplified resist derived from Arrhenius plot analysis. Two situation are considered: (a) before deblocking when TMAH penetration is prevented by strong hydrophobicity and (b) after deblocking. (From Itani, T., Itoh, K., and Kasama, K., *Proc. SPIE*, 1925, 388, 1993.)

plots of dissolution rate and log slope as a function of inhibitor concentration for a three-component PHOST chemically amplified resist [73]. Increasing both the protection ratio and the inhibitor concentration results in higher R_{max}/R_{min} contrast and DLS values. Strong surface inhibition effects can limit the practical levels. The optimum protection ratio from Figure 11.30 is on the order of 30%–35% with an inhibitor concentration of 3% PAG. Structure modification, molecular weight polydispersity, and polymer end groups can allow further improvements.

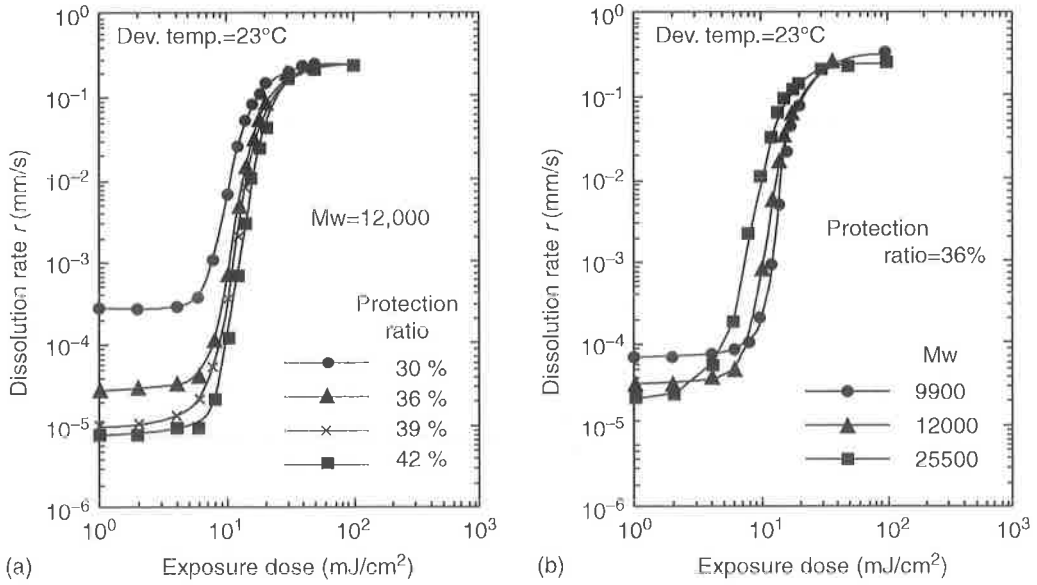

FIGURE 11.29
Development rate curves for a three-component positive DUV resist, which includes an additional dissolution inhibitor and various *t*-BOS protection levels and molecular weights. (From Itani, T., Iwasaki, H., Fujimoto, M., and Kasama, K., *Proc. SPIE*, 2195, 126, 1996.)

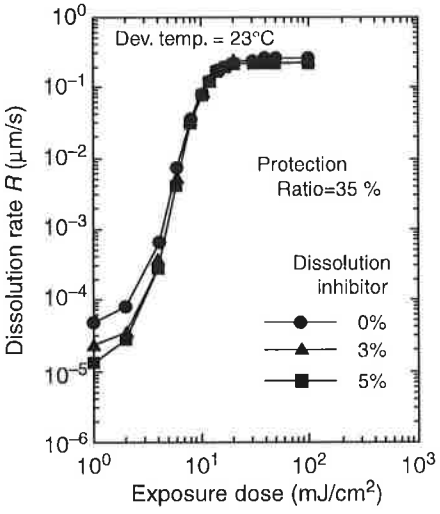

FIGURE 11.30
Plots of dissolution rate and log-slope plotted as a function of protection ratio for a three-component PHOST chemically resist. (From Itani, T., Iwasaki, H., Yoshin, H., Fujimoto, M., and Kasama, K., *Proc. SPIE*, 2438, 91, 1995.)

Preferential dissolution conditions for positive PHOST chemically amplified resists can be summarized. A high R_{max}/R_{min} contrast is desirable, but not so high as to result in severe resolution of sidewall standing waves (some low contrast behavior is desired to reduce sensitivity to small oscillations in intensity at threshold levels). Because R_{max} is primarily a function of the polymeric resin, maximizing the R_{max}/R_{min} dissolution contrast ratio generally involves reduction of unexposed resist erosion. As shown earlier, a ratio above 10,000 is desirable but probably no greater than 50,000 should be expected. A large DLS is more important and can be controlled to some extent by the resin molecular weight.

11.9 E_0 and CD Swing Curve

Coherent interference resulting from substrate reflectivity will result in a swing of intensity distributed within a resist film. This will correlate to variations in clearing dose (E_0) and CD throughout a resist layer. The swing in E_0 is dependent only on the coherent interference of radiation within the film and can be predicted on the basis of knowledge of the coupling efficiency between the resist and the exposure variation. The only requirement for predicting the E_0 swing is that the distribution and conversion efficiency of the sensitizer reaction be known, making it independent of resist dissolution characteristics. In other words, only the photospeed of the resist influences the E_0 swing. Figure 11.31 shows the relationship between the E_0 swing ratio and exposure clearing dose (E_0) for several resist systems [74]. The swing ratio has been calculated from Equation 11.11. Because higher bleaching efficiency leads to higher resist sensitivities, the relationship shown in Figure 11.31 makes sense from the standpoint of resist absorbance. Increased nonbleachable absorbance will lead to lower swing ratios, as can be demonstrated by adding a dye to a resist. Figure 11.32 is a plot of E_0 swing vs. exposure-independent resist absorbance (B parameter). As resist absorbance increases, swing decreases.

The independence of E_0 swing on resist dissolution, along with the ease with which E_0 values can be measured, makes it an effective method for resist coat characterization, as seen in Section 11.4. The swing in CD is not so straightforward because it is influenced by the resist process and dissolution properties. Resists process exposure latitude (or the

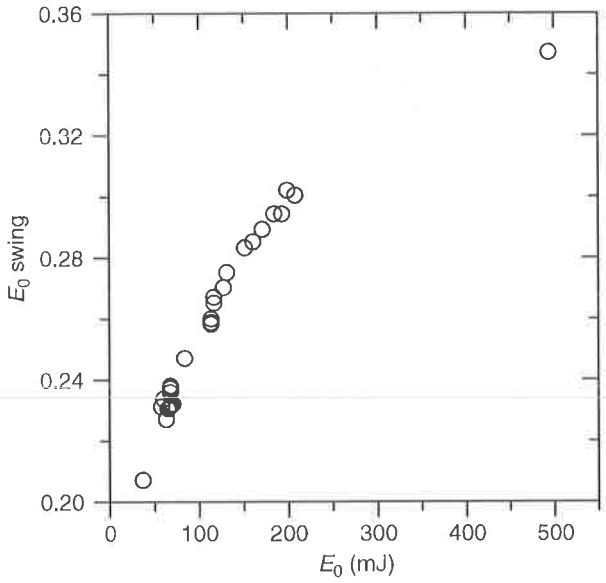

FIGURE 11.31
Plot of normalized E_0 vertical swing vs. E_0 for several hypothetical resist systems. (From Hansen, S.G., Hurdich, R.J., and Brzozowy, D.J., *Proc. SPIE*, 1925, 626, 1993.)

amount of the allowable over- or underexposure) can have a significant influence on CD swing, and can be predicted from the relationship

$$\text{CD swing} = \frac{E_0}{E_L^x}, \tag{11.17}$$

where E_L is exposure latitude and x is an empirically determined exponent, on the order of 2.5 for a reasonably fast photoresist.

Secondary swing effects are also present in a resist process. These include swings in resist contrast (γ) and surface contour effects. These secondary effects are a result of the spatial position of a standing wave node at the top surface of the resist. If there is a destructive interference node near the top surface of the resist, a surface induction effect

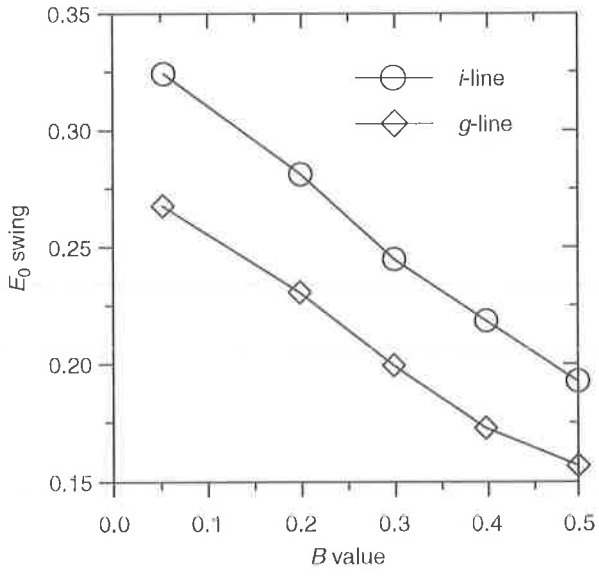

FIGURE 11.32
The effect or residual absorption (B parameter) on E_0 swing at constant sensitivity for g-line and i-line exposure. (From Hansen, S.G., Hurdich, R.J., and Brzozowy, D.J., *Proc. SPIE*, 1925, 626, 1993.)

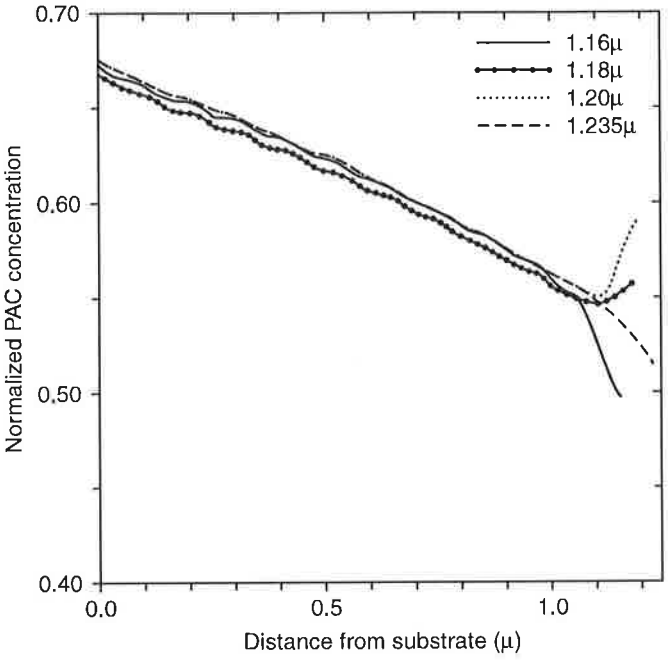

FIGURE 11.33
Calculated PAC distribution (at the mask edge) following PEB for four film thicknesses. (From Hansen, S.G., Hurdich, R.J., and Brzozowy, D.J., *Proc. SPIE*, 1925, 626, 1993.)

will result, leading to an increase in γ. Figure 11.33 shows how this can be manifested. At resist thicknesses slightly greater than those corresponding to an optimum maximum exposure (1.18 μm), PAC concentration is increased at the top surface of the resist, resulting in T-top formation. This results in a significant loss of linearity compared with the optimized condition. At thicknesses slightly less than 1.18 μm, there is a decrease in PAC concentration, resulting in top rounding. These surface effects occur at regular swing periods. The extent to which these secondary surface effects influence a resist process depends on how exposure requirements are affected. Surface effects influence clearing dose (E_0) more strongly than they influence dose to size ($E_{1:1}$) The exposure margin (EM), which is a ratio of these doses,

$$EM = \frac{E_{1:1}}{E_0}, \tag{11.18}$$

is a measure of the overexposure requirements for a resist and is a good indicator of mask linearity [75]. Surface-induced swing in E_0 leads to a corresponding swing in EM. Resists that demonstrate large surface induction effects during development are most susceptible to these secondary swing effects.

11.10 Postdevelopment Baking and Resists Treatment

Postdevelopment baking is often utilized to remove remaining casting solvent, developer, and water within the resist. Baking above the resist's T_g also improves adhesion of the resist to the substrate. Because photosensitivity is no longer required, the baking temperature can be elevated toward the solvent boiling point (T_b), effectively eliminating the solvent from the resist and allowing maximum densification. For a DNQ/novolac resist, any remaining DNQ can lead to problems in subsequent process steps. If the

still-sensitized resist is subjected to high-energy exposure (such as ion implantation), rapid release of nitrogen can result from radiolysis of DNQ. In densified resist films, the nitrogen cannot easily diffuse outward and may result in localized explosive resist popping that disperses resist particles on the wafer surface. Baking above the DNQ T_d after development is therefore desired to volatilize the PAC.

Novolac resins generally suffer from thermal distortion (during subsequent high-temperature processes) more than PHOST polymers. PHOSTs used for DUV resisters have T_g values on the order of 140°C–180°C; the T_g values for novolac resins are in the 80°C–120°C range. Elevated baking temperatures also result in oxidation and cross-linking of the novolac, producing more "thermoset" materials with flow temperatures higher than the original resist T_g (and less well defined). The temperatures required accomplish this, however, above the resist's T_g, thereby allowing the flow of patterned features in the process. Novolac resins with T_g values above 130°C are now commonly used and higher-T_g resists have been introduced [76].

To enhance the thermal properties of DNQ/novolac resists, the UV cross-linking properties of novolac can be utilized. Although the efficiency is quite low, novolac resin can be made to cross-link at DUV wavelengths. This is facilitated at high temperatures. The high optical absorbance of novolac at wavelengths below 300 nm (absorbance $\gg 1\ \text{mm}^{-1}$) prevents cross-linking to substantial depths. If patterned resist features are subjected to DUV exposure at temperatures above 150°C, a thermally stabilized surface crust can be formed. By elevating the temperature of the "DUV cure" process, oxidation of the bulk of the resist feature can be accomplished. The process is outlined in Figure 11.34. The now-networked resist feature can then withstand thermal processes up to 210°C without significant resist flow.

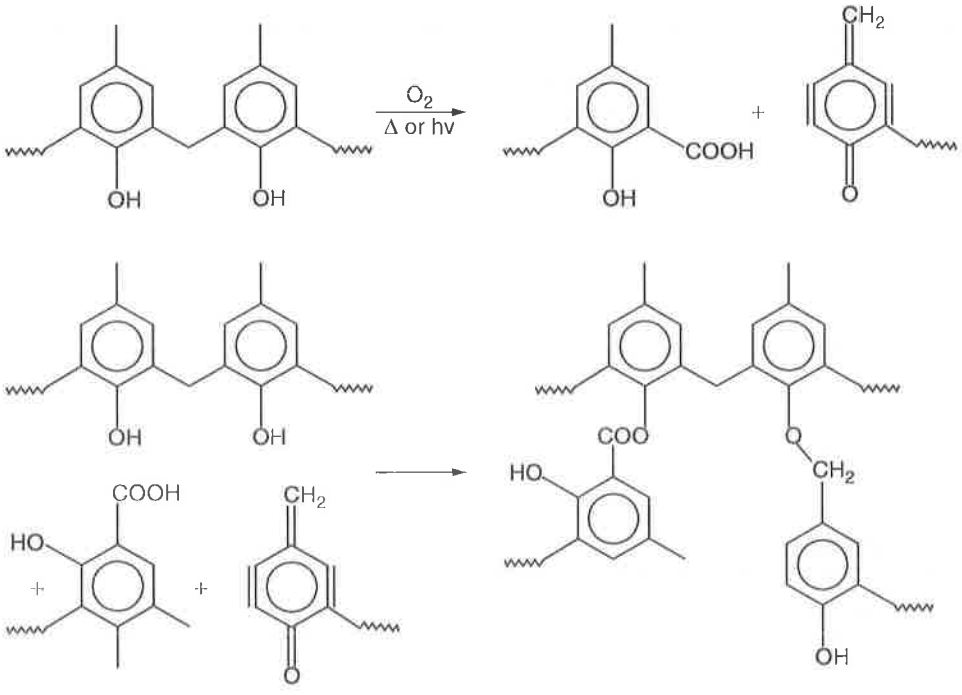

FIGURE 11.34
Radical reactions and oxidations induced in novolac from DUV curing. DUV hardening is effective in the presence of oxygen or with no oxygen (e.g., in nitrogen) through self-oxidation of novolac. Removal of DUV-cured novolac can be difficult and particulate contamination can occur from rapid nitrogen outgassing at high exposure levels.

11.11 Photoresist for 193-nm Lithography

As photolithography has progressed toward 130-nm design rules and beyond, the 193-nm ArF excimer laser has been employed as an enabling exposure source. The traditional phenolic polymers used for 248-nm and *g*/*i*-line application absorb heavily at 193 nm for this application. This is due to the structure of the phenolic ring that possesses a carbon–carbon double-bond which absorbs at wavelengths below 220 nm. Alternative platforms needed to be found that could retain suitable etch resistance and solubility but remain transparent at 193 nm. Resist systems based on polymethacrylates have consequently been developed. These systems can achieve adequate 193-nm transparency, high sensitivity, alkaline-develop-process compatibility, and good imaging properties for very low k_1 values [77]. The addition of alicyclic pendant groups have resulted in plasma etch resistance comparable to phenolic-based photoresists, leading to a generation of materials capable of supporting lithography well below the targeted 130-nm generations [78]. Most current 193-nm photoresists are based on five main platforms: (1) methacrylate copolymers with alicyclic pendant groups (MA), (2) ring-opening metathesis polymer (ROMP) with alicyclics in the main backbone, (3) cyclo-olefin addition polymers (CO), (4) alternating copolymers of cyclo-olefins with maleic anhydride (COMA), and (5) vinyl ether/maleic anhydride (VEMA). Three of these platforms have gained the most attention, specifically the MA, CO, and COMA approaches. The advantages and issues of these platforms are summarized in Table 11.2 [79].

The improvements in the etch resistance of these resist platforms have led to materials that are much more production worthy than the earliest formulations, but this remains an issue. The COMA resists exhibit the highest level of resistance but still do not compare to their 248-nm PHOST or *i*-line novolac counterparts. Integration of these materials may require the use of a hard-mask pattern transfer layer, typically silicon oxinitride (SiON). Such a layer can be designed and deposited as an underlying BARC, as described in Chapter 12. The most recent advances in these resists have led to their reduced sensitivity to the postexposure bake impact on CD control, which are approaching the levels of 248-nm PHOST materials. The issues associated with line slimming with SEM inspection will always remain an issue with acrylate polymers, as the basis of these systems is a scissioning polymer that undergoes volumetric losses with exposure to such high-energy sources. COMA resists are less sensitive to this effect, but the problems can be minimized when used with low SEM acceleration voltages. The acrylates and methacrylates have received recent attention because of their flexibility, both in terms of imaging performance

TABLE 11.2

Summary of the Performance Comparison for Three Major Photoresist Platforms for 193-nm Applications

Platform	Advantages	Issues
COMA	Etch resistance Mechanical rigidity	Transparency (moderate) Control water content
CO addition polymer	Transparency Excellent etch resistance Mechanical rigidity	Polymerization control Resin purification
MA acrylic Polymer	Transparency Design flexibility Excellent Adhesion	Etch resistance Mechanical rigidity Line slimming

and chemical synthesis. Because these polymers are free-radical type, they are simpler to formulate and modify to tailor imaging and processing properties. Their maturity, compared to the other systems, has also led to their adoption for most applications. In 2006, nearly 90% of all 193-nm resists sold fell into these two categories.

The main challenges with 193-nm resist technology will be those that are related to the continual shrinking of features size as very low k_1 lithography is pursued. As linewidths move below 90 nm and toward the 32-nm generations, the fundamental imaging limits of chemically amplified polymeric resists will eventually be reached. These 193-nm materials will be pushed to this doorstep.

11.12 Challenges for Current and Future Photoresists

In addition to the material attributes described above for the major 193-nm material platforms, there are at several fundamental challenges that will continue to require attention at every generational transition: resolution, outgassing, pattern collapse, and line-edge roughness (LER). Pattern collapse and LER may represent the largest near-term challenges with photoresist materials as the CD budget approaches the size scale of the polymers. The ultimate image resolution of chemically amplified resists will determine the longer range limits of these materials.

11.12.1 Image Resolution and Resist Blur

The application of chemical amplification has been the enabling factor in achieving highly sensitive photoresists for 248-nm and 193-nm applications. It was imperative in the early stages of DUV resist development that a route be identified by which the quantum efficiency of the photoresist materials could be increased to levels above 1.0. The acid-induced polymeric thermal deprotection and subsequent diffusion mechanisms that have allowed these resists to drive optical lithography for several decades will at some point lead to their detriment. This fundamental limit of these materials will be tied to the image blur or spread function that inherently results from this thermally activated deprotection and subsequent diffusion. As the targeted resolution for these materials approaches the physical blur function of diffusion, their usefulness will become limited.

The exposure of a chemically amplified resist generates a catalytic photoacid species. This photogenerated catalyst goes on to initiate a deprotection reaction and, because it is generally not consumed, induce the deprotection of many sites until it reaches an average catalytic chain length. This catalytic chain length may be several hundred atoms long, leading to a quantum efficiency (the number of reactions per photon absorbed) much larger than one. The fundamental limit to resolution is tied to this chain length because an image blur will result as the photoacid diffuses into unexposed resist regions. On a resolution scale where the physical diffusion is sufficiently smaller than the targeted geometry, an image bias results, where the printed line size is reduced. Photoacid size, exposure dose, mask bias, and bake process conditions can be used to compensate for this effect to some extent, but often a base additive will be employed to the resist formulation to decrease the diffusion of the acid. At the point where no acid diffusion is tolerable, the quantum efficiency must be reduced to one or below, leading to a non-chemically amplified photoresist system.

The spatial spread of an image in a chemically amplified photoresist is commonly called the *resist blur*. Through chemical kinetics simulations, the form of this blur function has been fit to a Lorentzian function, as shown in Figure 11.35 [80,81]. In a general

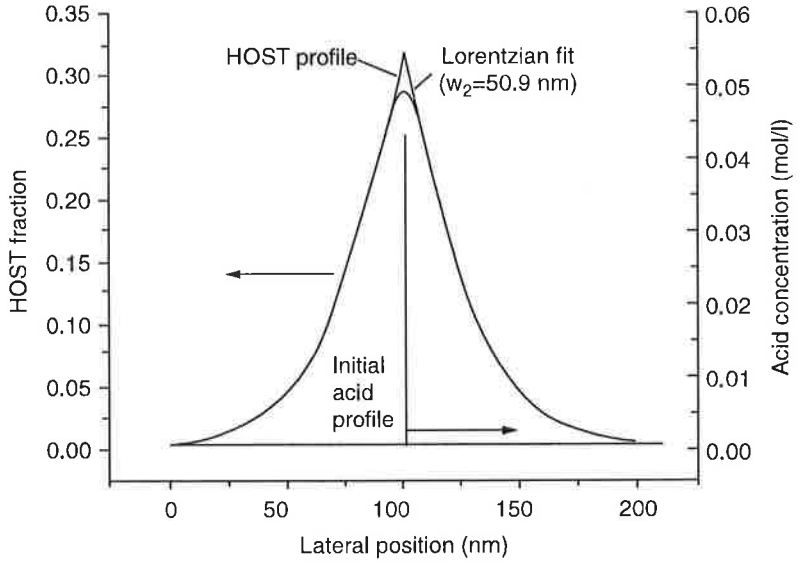

FIGURE 11.35
The resist blur function for a high activation energy resist, modeled by a Lorentzian function. The full width half maximum (FWHM) blur is on the order of 50nm. (From Brunner, T.A., *J. Vac. Sci. Technol. B*, 21, 2632, 2003.)

high-activation-energy resist, the resulting diffused resist blur after PEB may be on the order of 50 nm (FWHM) [82]. The blurring process can be approximated by convolution integrals, which have been modeled for some time. Fickian diffusion of an intensity profile in a photoresist has been used to account for acid diffusion, optical vibration, random aberration, and other effects [83]. The resist blur function such as the one in Figure 11.35 provides an additional level of understanding to the resolution limitations of a photoresist. A general rule of thumb can be used based on convolution requirements that image resolution is not possible when a blur function is larger than the image function itself. In other words, an image function can be made so small that it acts only as a probe for the blur function, constituting the resolution limiting aspect of the process. A blur value of 50 nm would therefore limit resolution to values of 65 nm or greater.

There are improvements that can be made to the resist blur function. The obvious one is the decrease in the catalytic amplification factor by limiting PEB or acid size. Though high-activation-energy resists exhibit blur values in the 40–60-nm range, values for low-activation-energy materials can be less than 20 nm. The ketal/acetal and carbonate/ester photoresists that fall into this category require little or no PEB to catalyze deprotection. Because the acid diffusion of these resist is reduced, blur can also be minimized [84]. The price paid for this can be detrimental as the benefits of resist blur to line-edge roughness are not carried out. Additionally, these platforms can produce excessive outgassing, leading to contamination of optical elements during the exposure process.

11.12.2 Photoresist Outgassing

The resist outgassing that has been and issue for vacuum lithography technologies (specifically electron beam and ion beam) has become an issue with optical lithography as well. When DNQ/novolac resists are exposed, nitrogen is released as a byproduct. Although this would limit the application of these resists for an immersion-lithography application, it has not posed a significant problem for conventional exposure in air. The chemically amplified resists used for 248 and 193 nm can be problematic, as byproducts can lead to

condensation on exposure optics, which dramatically reduces the lifetime of a projection lens. Careful control of the vapor pressure of solvent systems, photoacid generators, and additives can reduce these issues somewhat, as can the addition of radical scavengers to the resist formulation [85]. Although solvent outgassing can pose problems if a photoresist is not sufficiently baked near or above its glass transition temperature, careful bake-process design can nearly eliminate this from being a practical problem [86]. The level of outgassing resulting from acid-catalyzed deprotection immediately after exposure is a function of the photoacid generator and the polymer protecting group. Outgassing rates of 193-nm photoresists have been measured between 10^{11} and 10^{13} molecules cm^{-2} s^{-1}. The bulk of the species outgassed are protecting-group fragments and photoacid-generator fragments that can be reduced substantially when a high-activation resist platform is employed.

11.12.3 Line-Edge Roughness

Line-edge roughness (LER) is a primary concern for device geometries below 180 nm and becomes critical to understand and control for sub-90-nm generations. LER is different from linewidth roughness (LWR), which is related but is a measurement of the roughness effect on both sides of a feature. Although line thinning may not be indicated in a LER measurement, it would be measurable with LWR. LER and LWR of a patterned line are accumulations of variation from the photomask, exposure source, photoresist, and the resist-material stack. The metric used for LER is usually a 3σ measurement of variation, which generally should be no more than 5% of the critical dimension (CD) in the photoresist. This reduces the CD budget and will also be transferred to underlying layers during subsequent etch process steps. The photoresist contribution to LER has not been fully quantified but has been found to be related to several factors. Photoresist process conditions have been identified as an important factor in LER control [87], but molecular weight and distribution have been found to play a less significant role [88]. The dissolution of partially protected polymers influences LER only to a minor extent but the phase separation of protected and deprotected polymers can have a significant effect [89]. Polymer aggregates in the range of 23–30 nm in diameter can also lead to significant roughness [90]. Shot noise also becomes a contributor for small-pattern geometries. It would stand to reason that by increasing the acid diffusion length of a chemically amplified LER could be decreased. Although this is true, increasing the diffusion length to 20% of the targeted feature pitch value saturates the improvement; beyond that, only losses in image resolution and process latitude will result [91].

11.12.4 Resist Pattern Collapse

As the aspect ratio of photoresist features increases, so does their susceptibility to collapsing. This has especially become an issue for geometries below 130 nm where the stability of 193-nm and 248-nm resists may not withstand the mechanical stresses of spinning or the capillary forces of drying during process stages, as seen in Figure 11.36 [92–94]. Mechanical forces play a large role in the behavior, where the tops and centers of line features (furthest from the substrate) may experience attraction, resulting in contact after rinse and dry steps. The mechanical properties of the photoresist material, including the Young's modulus, residual strain, residual stress, coefficient of thermal expansion, and the glass transition temperature (T_g), will influence collapse. Several studies have determined the extent to which these factors influence patterning and allowed for the calculation of the

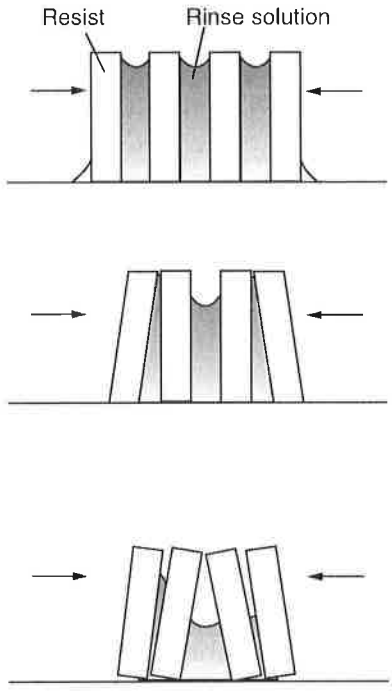

FIGURE 11.36
Resist pattern collapse for high aspect ratio line-space features.

effect [95–96]. The unbalanced capillary force surrounding a line (ΔF) can be determined as:

$$\Delta F = 2\gamma\left(\frac{1}{s_1} - \frac{1}{s_2}\right) HA \cos\theta, \tag{11.19}$$

where s_1 and s_2 represent the space regions surrounding the line, γ is the surface tension of the rinse fluid (where water is 72 mN/m), H is the film thickness, A is the line edge area, and θ is the contact angle of the rinse liquid. Uneven fluidic forces from rinse steps contribute most significantly to the collapse of resist lines. As a photoresist line becomes more compliant, lateral deflections can lead to the "shorting" of features from the top surface downward, which increases with aspect ratio. Collapse can also be influenced to a large extent by the adhesion of the photoresist to the substrate, feature profile (footing and undercut, as influenced by processing and reflection), pattern spacing, and pattern asymmetry. In general, symmetry on each side of a resist line feature will decrease the propensity for collapse as attractive forces are equilibrated, as can be seen from Equation 11.18, where s_1 and s_2 are equal. Asymmetry, such as the condition for the last line of a grouping, will increase the likelihood of collapse. Imaging conditions will also play a large role in pattern collapse, where best focus and exposure conditions provide the maximum image modulation conditions and the lowest susceptibility to mechanical failure. As excursions from ideal focus and exposure are explored, degradation will result [97]. As an example, the SEM images of Figure 11.37 are under a condition of defocus.

To overcome the problems associated with resist pattern collapse, several approaches have been introduced for the reduction of the surface tension and attractive capillary forces during rinse and drying steps. Work with alcohol-based rinses followed by supercritical CO_2 (SCC) drying has shown promise, where surface tension vanishes in the supercritical phase [98]. Problems with the recondensation of water during the SCC drying process and the need for high-pressure chambers may present challenges. Alternative processes involving SCC as a solvent and development media have also been

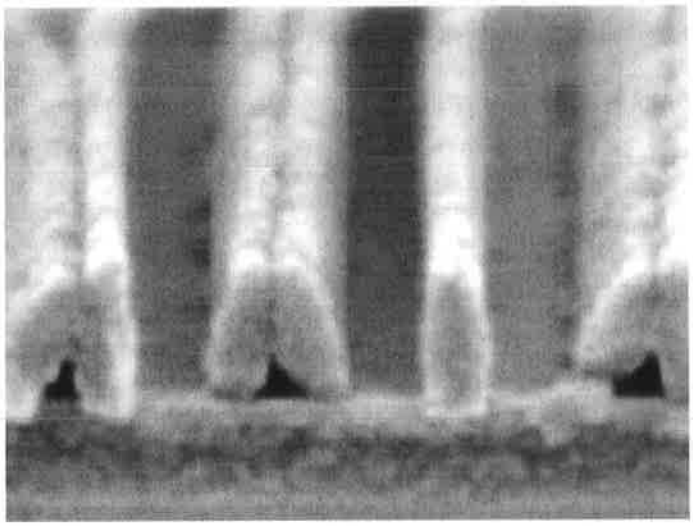

FIGURE 11.37
Pattern collapse for resist features with defocus, which increases the susceptibility for failure.

introduced, but their practicality relies on the development of processing and tooling for their application [99]. A more adaptable solution to the problem may be the introduction of surfactants during the final rinse stage of processing [100]. Because capillary forces scale with the surface tension of the resist liquid and contact angle, rinse liquids with a low surface tension can minimize the unbalanced capillary forces. The challenge with rinse agents and surfactants is their compatibility with the variety of resist chemistries employed for sub-130-nm imaging. A thorough screening of materials for compatibility is required prior to implementation. An ideal strategy to reduce collapse problems is the design of resist materials so that the surface tension is optimized for use with water rinsing.

11.13 Photoresist Issues for Immersion Lithography

As immersion lithography is employed for use at 193 nm, several issues arise that are unique to imaging in a fluidic environment. Some of these are addressed in Chapter 3, Section 3.10. Additional process concerns include the leaching or extraction of resist components into the immersion fluid, the diffusion of the immersion fluid into the resist matrix, and the timescales of these processes related to imaging and subsequent mechanisms.

The leaching of PAG and base additives from a photoresist has been shown to be a surface phenomenon where a small volume of molecules are extracted, on the order of 3%–5% for a 200-nm film [101,102]. The leaching occurs quickly, equilibrating after the first 10 s of contact between the photoresist and the fluid (where water has been most extensively studied) [103]. The simplest model assumes that the leaching of a PAG is a function of the number of molecules at the surface, which is quite adequate for understanding the mechanisms involved. Resist formulations optimized for use with water-immersion imaging are needed to minimize this leaching, otherwise top-coat materials will be needed as a barrier layer between the photoresist and the fluid [104]. As water is diffused into a photoresist film, it swells and experiences an increase in thickness. Using quartz crystal microbalance and optical reflectance techniques, the water uptake of a photoresist film during contact with water has been measured [105]. During the first 30 s of exposure

to water, up to 4 parts per thousand can be carried into the photoresist film [106]. Despite the significant extraction of resist components into the immersion fluid and the relatively large amount of water driven into the photoresist film, the impact to imaging with the existing 193-nm resist platforms have been surprisingly minimal. Using interferometric immersion lithography for imaging various fluids and resists, a large number of materials have been tested and have achieved resolution well below 45 nm [107,108]. Unlike the challenges that have been involved with the transitional requirements for photoresist materials with the changing of exposure wavelength, there has not been a need for a new class of materials for 193-nm water-immersion lithography. New schemes will become necessary as the resolution scale is pushed beyond the fundamental image capabilities of polymeric chemically amplified resist platforms.

References

1. L.F. Thompson, C.G. Wilson, and M.J. Bowden. 1994. *Introduction to Microlithography,* Washington, DC: American Chemical Society.
2. W. Moreau. 1988. *Semiconductor Lithography,* New York: Plenum.
3. R. Dammel. 1993. Diazonapthoquinone-Based Resists, *Chapter 5,* 5, Bellingham, WA: SPIE.
4. W. Moreau. 1988. *Semiconductor Lithography,* New York: Plenum, p. 49.
5. L. Katzisyma. 1966. *Russ. Chem. Rev.*, **35:** 388.
6. S. Asaumi, M. Futura, and A. Yokota. 1992. *Proc. SPIE*, **1672:** 616.
7. W.D. Hinsberg et al. 1993. *Proc. SPIE*, **1925:** 43.
8. W. Huang et al. 1994. *Proc. SPIE*, **2195:** 37.
9. O. Nalamasu et al. 1995. ACS Symp, *Ser.*, **614:** 4.
10. H. Roschert et al. 1992. *Proc. SPIE*, **1672:** 33.
11. D.J.H. Funhoff, H. Binder, and R. Schwalm. 1992. *Proc. SPIE*, **1672:** 46.
12. O. Nalamasu et al. 1992. *J. Vac. Sci. Technol. B*, **10:**6, 2536.
13. H. Ito et al. 1994. *J. Photopoly. Sci. Technol.*, **7:** 433.
14. W. Conley et al. 1996. *Proc. SPIE*, **2724:** 34.
15. S.A. McDonald. 1991. *Proc. SPIE*, **1466:** 2.
16. J.H. van Zanten, W.E. Wallace, and W.L. Wu. 1996. *Phys. Rev. E.*, **53:** R2053.
17. D. Lyons and B.T. Beauchemin. 1995. *Proc. SPIE*, **2438:** 726.
18. D.E. Bornside, C.W. Macosko, and L.E. Scriven. 1987. *J. Imag, Tech.*, **13:** 123.
19. D. Meyerhofer. 1978. *J. Appl. Phys.*, **49:**7, 3993.
20. H. Fujita. 1961. *Adv. Polym. Sci.*, **3:** 1.
21. J.S. Vrentas. 1977. *J. Polym. Sci. Polym. Phys. Ed.*, **15:** 403.
22. L. Pain, C. LeCornec, C. Roilio, and P.J. Paniez. 1996. *Proc. SPIE*, **2724:** 100.
23. V. Rao, W.D. Hinsberg, C.W. Frank, and R.F.W. Pease. 1994. *Proc. SPIE*, **2195:** 596.
24. C.W. Frank, V. Rao, M.M. Despotopoulou, R.F.W. Pease, W.D. Hinsberg, R.D. Miller, and J.F. Rabolt. 1996. *Science*, **273:** 912.
25. L. Schlegel, T. Ueno, N. Hayashi, and T. Iwayanagi. 1991. *J. Vac. Sci. Technol. B*, **9:** 278.
26. B. Beauchemin, C.E. Ebersol, and I. Daraktchiev. 1994. *Proc. SPIE*, **2195:** 613.
27. T.E. Salamy et al.1 1990. *Proc. Electrochem. Soc.*, **90:**1, 36.
28. K.R. Dean, R.A. Carpio, and G.K. Rich. 1995. *Proc. SPIE*, **2438:** 514.
29. J. Chun, C. Bok, and K. Baik. 1996. *Proc. SPIE*, **2724:** 92.
30. E. Fields, C. Clarisse, and P.J. Paniez. 1996. *Proc. SPIE*, **2724:** 460.
31. P.J. Paniez, C. Rosilio, B. Monanda, and F. Vinet. 1994. *Proc. SPIE*, **2195:** 14.
32. R. Sinta, G. Barclay, T. Adams, and P. Medeiros. 1996. *Proc. SPIE*, **2724:** 238.
33. P.J. Paniez, G. Festes, and J.P. Cholett. 1992. *Proc. SPIE*, **1672:** 623.
34. M. Koshiba, M. Murata, M. Matsui, and Y. Harita. 1988. *Proc. SPIE*, **920:** 364.
35. H. Ito et al. 1995. *Proc. SPIE*, **2438:** 53.
36. F.H. Dill et al. 1975. *IEEE Trans. Electr. Dev.*, **ED-22:** 440.

37. R. Dammel. 1993. *Diazonapthoquinone-Based Resists*, Bellingham, WA: SPIE Pres, p. 19.
38. J. Sturdevant, W. Conley, and S. Webber. 1996. *Proc. SPIE*, **2724:** 273.
39. J.M. Shaw and M. Hatzakis. 1978. *IEE Trans. Electr. Dev.*, **ED-25:** 425.
40. T. Brunner. 1991. *Proc. SPIE*, **1463:** 297.
41. J. Sturdevant, S. Holmes, and P. Rabidoux. 1992. *Proc. SPIE*, **1672:** 114.
42. M.A. Toukhy and S.G. Hansen. 1994. *Proc. SPIE*, **2195:** 64.
43. T. Tanabe, Y. Kobayashi, and A. Tsuji. 1996. *Proc. SPIE*, **2724:** 61.
44. L. Pain, C. Le Cornec, C. Rosilio, and P.J. Paniez. 1996. *Proc. SPIE*, **2724:** 100.
45. K. Überreiter and F. Asmussen. 1962. *J. Polym. Sci.*, **57:** 187.
46. A.E. Novembre and M.A. Hartney. 1985. *Proc. SPE Photopolym. Conf.*, New York: Ellenvile.
47. J.P. Huang, T.K. Kwei, and A. Reiser. 1989. *Proc. SPIE*, **1086:** 74.
48. A. Reiser. 1989. *Photoreactive Polymers*, New York: Wiley Interscience, pp. 211–223.
49. H. Shin, T. Yeu, and A. Reiser. 1994. *Proc. SPIE*, **2195:** 514.
50. K. Honda, A. Blakeney, and R. Hurditch. 1993. *Proc. SPIE*, **1925:** 197.
51. T. Itani, K. Itoh, and K. Kasama. 1993. *Proc. SPIE*, **1925:** 388.
52. K.L. Konnerth and F.H. Dil. 1975. *IEEE Trans. Electr. Dev.*, **ED-22:** 453.
53. S.D. Chowdhury, D. Alexander, M. Goldman, A. Kukas, N. Farrar, C. Takemoto, and B.W. Smith. 1995. *Proc. SPIE*, **2438:** 659.
54. For instance, the Perkin Elmer Development Rate Monitor (DRM).
55. R.A. Arcus. 1986. *Proc. SPIE*, **631:** 124.
56. R.R. Dammel et al. 1994. *Proc. SPIE*, **2195:** 542.
57. S. Shimomura, H. Shimada, R. Au, M. Miyawaki, and T. Ohmi. 1993. *Proc. SPIE*, **1925:** 602.
58. G. Flores and J. Loftus. 1992. *Proc. SPIE*, **1672:** 328.
59. C.L. Henderson et al. 1996. *Proc. SPIE*, **2724:** 481.
60. C. Henderson et al. 1996. *Proc. SPIE*, **2724:** 481.
61. K. Honda, A. Blakeney, and R. Hurdith. 1993. *Proc. SPIE*, **1925:** 197.
62. C.M. Garza, C.R. Szmanda, and R.L. Fischer. 1988. *Proc. SPIE*, **920:** 321.
63. V. Marriott. 1983. *Proc. SPIE*, **394:** 144.
64. W. Moreau. 1988. *Semiconductor Lithography*, New York: Plenum Press, Ch. 10.
65. W.M. Moreau, A.D. Wilson, K.G. Chiong, K. Petrillo, and F. Hohn. 1988. *J. Vac Sci. Technol. B*, **6:** 2238.
66. E. Fadda, G.M. Amblard, A.P. Weill, and A. Prola. 1994. *A. Proc. SPIE*, **2195:** 576.
67. T. Yoshimura, E. Murai, H. Shiraishi, and S. Okazaki. 1990. *J. Vac. Sci. Technol. B*, **6:** 2249.
68. N. Damarakone, P. Jaenen, L. Van den Hove, and R. Hurditch. 1990. *J., Proc. SPIE*, **1262:** 219.
69. T. Itani, K. Itoh, and K. Kasama. 1993. *Proc. SPIE*, **1925:** 388.
70. J.W. Thackeray et al. 1989. *Proc. SPIE*, **1086:** 34.
71. O. Nalamasu et al. 1990. *Proc. SPIE*, **1262:** 32.
72. T. Itani, H. Iwasaki, M. Fujimoto, and K. Kasama. 1994. *Proc. SPIE*, **2195:** 126.
73. T. Itani, H. Iwasaki, H. Yoshin, M. Fujimoto, and K. Kasama. 1995. *Proc. SPIE*, **2438:** 91.
74. S.G. Hansen, R.J. Hurdich, and D.J. Brzozowy. 1993. *Proc. SPIE*, **1925:** 626.
75. S.G. Hansen and R.H. Wang. 1993. *J. Electrochem. Soc*, **140:** 166.
76. M.A. Toukhy, T.R. Sarubbi, and D.J. Brzozowy. 1991. *Proc. SPIE*, **1466:** 497.
77. R. Allen et al. 1993. *Solid State Technol.*, **36:** 11, 53–62.
78. S. Takechi et al. 1992. *J. Photopol. Sci. Technol.*, **5:** 439.
79. K. Ronse. 2001. *Future Fab International*, **10**.
80. F.A. Houle, W.D. Hinsberg, M.I. Sanchez, and J.A. Hoffnagle. 2002. *J. Vac. Sci. Technol. B*, **20:** 924.
81. J.A. Hoffnagle, W.D. Hinsberg, M.I. Sanchez, and F.A. Houle. 2002. *Optics Letters*, **27:** 1776.
82. T.A. Brunner. 2003. *J. Vac. Sci. Technol. B*, **21:** 2632.
83. T.A. Brunner and R.A. Fergusen. *Proc. SPIE*, **2726:** 198.
84. G.M. Walraff, D.R. Medeiros, M. Sanchez, K. Petrillo, and W.S. Huang. 2004. *J. Vac. Sci. Technol. B*, **22:** 3479.
85. O. Nalamasu and A.H. Gabor. 2000. *Future Fab International*, **8:** 159–163.
86. R.R. Kunz and D.K. Downs. 1999. *J. Vac. Sci. Technol. B*, **17:** 3330.

87. S. Palmateer, S. Cann, J. Curtin, S. Doran, L. Ericksen, A. Forte, R. Kunz, T. Lyszczarz, and M. Stern et al. 1998. *Proc. SPIE*, **3333:** 634–642.
88. S. Masuda, X. Ma, G. Noya, and G. Pawlowski. 2000. *Proc. SPIE*, **3999:** 253.
89. Q. Lin, D. Goldfarb, M. Angelopoulos, S. Sriam, and J. Moore. 2001. *Proc. SPIE*, **4345:** 78.
90. T. Yamaguchi, H. Namatsu, M. Nagese, K. Yamazaki, and K. Kurihara. 1997. *J. Photopoly. Sci. Technol.*, **10:** 635.
91. U. Okoroanyanwu and J.H. Lammers. 2004. *Future Fab International*, **17**.
92. A.M. Goethals et al. 2001. *J. Photopol. Sci. Technol.*, **3:** 333.
93. W.D. Domke et al. 1999. *Proc. SPIE*, **3999:** 139.
94. S. Mori, T. Morisawa, N. Matsuzawa, Y. Kaimoto, M. Endo, T. Matsuo, M. Sasago. *J. Vac. Sci. Technol. B*, **16**: 3744.
95. L. Que and Y.B. Gianchandania. 2000. *J. Vac. Sci. Technol. B*, **18:** 3450.
96. G. Czech, E. Richter, and O. Wunnicke. 2002. *Future Fab International*, **12.**
97. O. Wunnickea, A. Henniga, K. Grundkeb, M. Stammb, and G. Czecha. 2002. *Proc. SPIE*, **4690:** 332.
98. J. Simons, D. Goldfarb, M. Angelopoulos, S. Messick, W. Moreau, C. Robinson, J. De Pablo, and P. Nealey. 2000. *Proc. SPIE*, **4345:** 19–29.
99. C.L. McAdams et al. 2000. *Proc. SPIE*, **4345:** 327–334.
100. S. Hien, G. Rich, G. Molina, H. Cao, and P. Nealy. 2002. *Proc. SPIE*, **4690:** 254.
101. W. Hinsberg, G. Wallraff, C. Larson, B. Davis, V. Deline, S. Raoux, D. Miller, F. Houle, J. Hoffnagle, M. Sanchez et al. 2004. *Proc. SPIE*, **5376:** 21–33.
102. M. Yoshida, K. Endo, K. Ishizuka, and M. Sato. 2004. *J. Photopol. Sci. Technol.*, **17:** 603.
103. R.R. Dammel, F.M. Houlihan, R. Sakamuri, D. Rentkiewicz, and A. Romano. 2004. *J. Photopol. Sci. Technol.*, **17:**4, 587–602.
104. R. Dammel, G. Pawlowski, A. Romano, F. Houlihan, W.K. Kim, and R. Sakamuri. 2005. *Proc. SPIE*, **5753:** 95.
105. W. Hinsberg, F. Houle, H. Ito, K. Kanzawa, S-W. Lee. 2003. in *Proceedings of the 13th International Conference on Photopolymers*, Society of Plastics Engineers.
106. W. Hinsberg, G. Walraff, C. Larson, B. Davis, V. Deline, S. Raoux, D. Miller, F. Houle, J. Hoffnagle, M. Sanchex et al. 2005. *Proc. SPIE*, **5376:** 21.
107. B.W. Smith, A. Bourov, Y. Fan, L. Zavyalova, N. Lafferty, and F. Cropanese. 2004. *Proc. SPIE*, **5377:** 273–282.
108. A. Raub and S. Brueck. 2003. *Proc. SPIE*, **5040:** 667.